Redefining De Novo Gammaherpesvirus Infection Through High-Dimensional, Single-Cell Analysis of Virus and Host

Jennifer N. Berger[1], Bridget Sanford[2], Abigail K. Kimball[3], Lauren M. Oko[1], Rachael E. Kaspar[3], Brian F. Niemeyer[1], Kenneth L. Jones[4], Eric T. Clambey[3]*, Linda F. van Dyk[1,5]*

Affiliations

[1] Department of Immunology and Microbiology, University of Colorado Anschutz Medical Campus | Aurora, CO, 80045, USA

[2] Department of Pediatric Oncology, University of Colorado Anschutz Medical Campus | Aurora, CO, 80045, USA

[3] Department of Anesthesiology, University of Colorado Anschutz Medical Campus | Aurora, CO, 80045, USA

[4] Department of Cell Biology, University of Oklahoma Health Sciences Center | Oklahoma City, OK, 73104, USA

[5] Lead Contact

* Co-corresponding authors. Address correspondence and reprint requests to Dr. Eric Clambey (Eric.Clambey@cuanschutz.edu) and Dr. Linda van Dyk (Linda.VanDyk@cuanschutz.edu)

Running title: Single-cell analysis of de novo gammaherpesvirus infection

ORCIDs:

https://orcid.org/0000-0002-7546-2758 (J.N.B.); 0000-0002-2173-0198 (B.S.); 0000-0002-9831-386X (A.K.K.); 0000-0002-7125-7036 (L.M.O.); 0000-0002-1181-7919 (R.E.K.); 0000-0002-2020-2238 (B.F.N); 0000-0003-4572-3651 (K.L.J); 0000-0002-7972-9544 (E.T.C.); 0000-0003-2662-5554 (L.F.v.D.).

SUMMARY

Virus infection is frequently characterized using bulk cell populations. How these findings correspond to infection in individual cells remains unclear. Here, we integrate high-dimensional single-cell approaches to quantify viral and host RNA and protein expression signatures using de novo infection with a well-characterized model gammaherpesvirus. While infected cells demonstrated genome-wide transcription, individual cells revealed pronounced variation in gene expression, with only 9 of 80 annotated viral open reading frames uniformly expressed in all cells, and a 1000-fold variation in viral RNA expression between cells. Single-cell analysis further revealed positive and negative gene correlations, many uniquely present in a subset of cells. Beyond variation in viral gene expression, individual cells demonstrated a pronounced, dichotomous signature in host gene expression, revealed by measuring host RNA abundance and post-translational protein modifications. These studies provide a resource for the high-dimensional analysis of virus infection, and a conceptual framework to define virus infection as the sum of virus and host responses at the single-cell level.

HIGHLIGHTS

- CyTOF and scRNA-seq identify wide variation in gene expression between infected cells.
- Host RNA expression and post-translational modifications stratify virus infection.
- Single cell RNA analysis reveals new relationships in viral gene expression.
- Simultaneous measurement of virus and host defines distinct infection states.

INTRODUCTION

Gammaherpesviruses (γHVs) are a subfamily of the *Herpesviridae* characterized by their ability to establish latency in lymphoid cells and their association with numerous malignancies (Barton et al., 2011; Cesarman, 2014; Zamora, 2011). The γHVs include the human viruses Kaposi's sarcoma-associated herpesvirus (KSHV, or human herpesvirus 8) and Epstein-Barr virus (EBV), and murine gammaherpesvirus 68 (MHV68 or γHV68; ICTV nomenclature, *murid herpesvirus 4*, MuHV-4), a model system for its human virus counterparts (Barton et al., 2011; Dong et al., 2017; Virgin et al., 1997). MHV68 provides a genetically tractable system, capable of inducing a range of outcomes *in vitro* and *in vivo* (Barton et al., 2011; Forrest and Speck, 2008; Suarez and van Dyk, 2008).

Like other herpesviruses, the MHV68 lifecycle is characterized by two major stages: latent and lytic infection (Pellett and Roizman, 2013). During latent infection, viral gene expression is limited, with no *de novo* viral replication (Pellett and Roizman, 2013). While latent γHV infection is associated with lifelong infection and malignancies, the γHVs critically rely on lytic infection for virus replication and transmission between hosts. Lytic infection is characterized by robust viral gene expression and the production of new infectious virions. The conventional view of lytic infection is that of a synchronous cascade of gene expression that results in genome-wide transcription. The paradigm for lytic gene expression was established in bulk cell populations, stratifying viral gene expression into three broad categories: immediate-early (IE), early (E), and late (L) gene expression (Johnson et al., 2010; Pellett and Roizman, 2013; Rochford et al., 2001). IE genes are expressed in the absence of new viral protein synthesis, E genes require new viral protein synthesis but do not require new viral DNA synthesis, and L genes require new viral DNA synthesis (Ahn et al., 2002; Ebrahimi et al., 2003; Johnson et al., 2010; Martinez-Guzman et al., 2003; Pellett and Roizman, 2013). Lytic gene expression can also be

stratified by kinetic class, affording a revised perspective on viral gene expression (Cheng et al., 2012).

The advent of high-throughput, single-cell based methods has revealed a more complex picture of herpesvirus infection, from latent infection (Messinger et al., 2019; Oko et al., 2019; Shnayder et al., 2018), to lytic infection (Drayman et al., 2019; Oko et al., 2019; Wyler et al., 2019), reactivation from latency (Adang et al., 2006; Oko et al., 2019) and viral tropism (Sen et al., 2014). Recently, we identified unanticipated heterogeneity between infected cells during lytic infection, with wide variance in viral gene expression, from cells with robust viral gene expression to cells with little to no detectable expression of either viral non-coding RNAs or mRNAs (Oko et al., 2019). These studies suggest that lytic infection may be more heterogeneous in individual cells than the perspective revealed by analysis of bulk populations.

Though stages of infection are defined based on viral gene expression, lytic infection is also associated with profound alterations in host gene expression. First, many herpesviruses, including KSHV, EBV, MHV68, varicella zoster virus (VZV), and Herpes simplex virus (HSV), induce widespread degradation of host RNAs (i.e. host shutoff) during lytic infection, a phenomenon associated with decreased expression of cellular housekeeping genes in either bulk cell populations (Glaunsinger, 2015; Smiley, 2004; Waterboer et al., 2002) or individual cells (Oko et al., 2019). Viruses have also evolved diverse mechanisms to manipulate host processes (e.g. cell cycle, apoptosis, protein synthesis and signal transduction) (Chang et al., 2016). For example, the ORF36 gene of MHV68 and EBV encodes a viral kinase that phosphorylates H2AX, a proximal marker of the DNA damage response, to facilitate viral replication (Tarakanova et al., 2007). Recent studies have further demonstrated that the EBV and KSHV ORF36 homologs target additional host proteins including SAMHD1 and S6K to impact virus restriction and protein synthesis, respectively (Bhatt et al., 2016; Zhang et al., 2019). These studies emphasize that measuring host processes commonly targeted by multiple viruses [including host shutoff (Glaunsinger, 2015), DNA damage responses

(Weitzman and Fradet-Turcotte, 2018) and innate signaling (Lee et al., 2015)], may provide an important, complementary strategy to define viral infection.

Here we provide a resource to redefine lytic infection from a single-cell perspective, using cytometry by time-of-flight (CyTOF, or mass cytometry) and single cell RNA-seq to achieve high-dimensional, single-cell analysis of viral and host gene expression. These studies reveal: i) the highly variable nature of viral gene expression between individual cells, with only a small subset of genes expressed across all cells, ii) the utility of measuring host parameters as a discriminator to identify infection state, and iii) new insights into infection and gene expression relationships, previously obscured by bulk cell analysis.

RESULTS

CyTOF analysis identifies a distinct protein expression profile for virally-infected cells.

Recently, we discovered significant variability in viral gene expression between cells during MHV68 infection (Oko et al., 2019). These studies identified a prominent fraction of cells with limited viral gene expression, a phenomenon that could arise due to asynchronous infection, infection with restricted viral gene expression (e.g. latency), or cells resistant to infection. To define the complexity of virus infection in productively infected cells, we established a system to purify cells based on expression of the MHV68 latency-associated nuclear antigen (LANA) protein, a viral gene product expressed during lytic and latent infection (Rochford et al., 2001). NIH 3T12 fibroblasts, a highly permissive cell line for MHV68 lytic infection, were infected with a wild-type MHV68 recombinant expressing a LANA::β-lactamase gene fusion (WT MHV68.LANAβlac), followed by FACS purification (Diebel et al., 2015; Nealy et al., 2010) and high-dimensional single-cell analysis using CyTOF and single cell RNA-sequencing (scRNA-seq).

First, we analyzed virally-infected cells by CyTOF, to obtain a high-dimensional single-cell analysis of protein expression (Kimball et al., 2018). NIH 3T12 fibroblasts were harvested at 16 hours post-infection (hpi), a time at which no cytopathic effect or new progeny virus is released, and sort purified into LANAβlac+ (LANA+) and LANAβlac- (LANA-) fractions (Figure S1A). On average, >94% of cells were LANA+ at this time, indicating active virus infection in the vast majority of cells (Niemeyer et al., 2018). Mock-infected 3T12 cells were purified in parallel. To ensure robust cross-comparison between these populations, each sample was subjected to isotopic palladium-based barcoding, pooled together, stained with a panel of 23 isotopically-labelled antibodies, with samples collected on a Helios mass cytometer (Figure 1A). Mock-infected, LANA+ and LANA- cells had pronounced differences in clustering and protein expression profiles (Figure S1B-D). LANA+ cells robustly expressed the virally-

encoded regulator of complement activation (vRCA) protein (Kapadia et al., 1999) and phosphorylated histone H2AX (pH2AX), a target of the ORF36 viral kinase (Tarakanova et al., 2007). LANA+ cells further showed increased expression of cell surface proteins (CD9, MHC I) and cell cycle proteins (Ki-67, phosphorylated Rb [Serine 807/S811]), with modest induction of signal transduction pathways (activated beta-catenin, pERK1/2, p-p38, pStat1, pStat3, pAKT and pS6) compared to both LANA- and mock-infected populations (Figure S1C-D). These data indicate that at the population level, LANA+ cells have a distinct protein expression signature relative to mock-infected and LANA- cells.

Next we quantified the diversity of cellular phenotypes between LANA+ and LANA- cells. When we applied PhenoGraph, an unsupervised clustering algorithm (Levine et al., 2015), we identified 14 phenotypes across LANA+, LANA-, and mock-infected populations (Figure 1B). The frequency of phenotypic clusters varied widely between LANA+ and LANA- populations (Figure 1C), with 3 clusters exclusively present among LANA+ cells, 5 clusters uniquely present among LANA- cells, and 6 clusters containing both LANA+ and LANA- cells (Figure 1C). Clusters exclusively present among LANA+ cells (clusters 1-3, at the bottom of Figure 1C) were characterized by maximal expression of vRCA and pH2AX, and increased expression of pRB, pERK1/2, pAKT, and pS6 relative to other cell clusters (Figure 1C). Expression of other parameters, including CD9, CD29, CD44, CD63, Ki-67 and IkBα did not strictly correlate with either LANA+ or LANA- cells, indicating that these proteins were not solely regulated as a function of virus infection (Figure 1C). While high expression of vRCA and pH2AX was a strong discriminator between clusters exclusively in LANA+ versus LANA- events, approximately half of LANA+ events expressed low levels of either vRCA or pH2AX, overlapping with LANA- cells (Figure 1C-D). These data indicate that while many cells expressing the LANAβlac fusion protein had increased virus and host protein expression, there was a substantial fraction of LANA+ cells that could not be readily distinguished from LANA-

cells (clusters colored purple, Figure 1D). These data further identify phosphorylation of H2AX (i.e. pH2AX) as a robust marker of virus-induced phenotypic changes at the single-cell level.

LANA+ cells show heterogeneous protein and post-translational modifications during lytic infection.

To better understand phenotypic heterogeneity among cells with active viral gene expression (i.e. LANA+ cells), we quantified phenotypic diversity among a large number of LANA+ cells, clustering cells based on expression of nine cell surface-expressed proteins (BST2, CD9, CD29, CD44, CD63, Ly6A/E, Ly6C, MHCI, and vRCA). This focused clustering analysis identified 15 phenotypic clusters within LANA+ cells, which were then visually inspected based on vRCA, pH2AX, Ly6C, and BST2 expression (Figure 2A-C). LANA+ cells could be subdivided into cells with high and low viral gene expression, with vRCA and pH2AX expression tightly overlapping. In contrast, Ly6C and BST2 protein expression was variable across $vRCA^{high}$ $pH2AX^{high}$ and $vRCA^{low}$ $pH2AX^{low}$ cell fractions, indicating that these proteins did not simply correlate with virus infection (Figure 2B-C). Stratification of LANA+ cells into $pH2AX^{high}$ and $pH2AX^{low}$ subsets (Figure S2A) demonstrated that $pH2AX^{high}$ cells had increased expression of vRCA, MHC class I, and multiple phosphorylation-dependent modifications including pRb, active β-catenin, pERK1/2, pStat1 and pAKT compared to $pH2AX^{low}$ cells (Figure 2D). $pH2AX^{high}$ cells also had modestly decreased expression of CD9, CD29, Ly6A/E, Ly6C and IkBα relative to $pH2AX^{low}$ events (Figure 2D). Consistent with the tight correlation between vRCA and pH2AX expression, LANA+ $vRCA^{high}$ cells had increased expression of pH2AX, MHC class I, pRb, active β-catenin, pERK1/2, pStat1 and pAKT compared to $vRCA^{low}$ cells and modestly reduced IkBa expression (Figure S2B-E). These studies indicate that vRCA and pH2AX are strong markers of progressive infection among LANA+ events, with phosphorylated Rb a robust secondary marker associated with a

185 pH2AX^{high} vRCA^{high} phenotype. These results further indicate that heterogeneous progression
186 through infection can be revealed by monitoring host protein expression at the single-cell level.
187
188 *MHV68-infected cells with a pH2AX^{high} vRCA^{high} cell phenotype express high viral mRNA and*
189 *low host actin RNA.*
190 We next investigated how pH2AX and vRCA expression corresponded with viral and
191 host RNA expression at the single-cell level, using the PrimeFlow methodology to
192 simultaneously measure protein and RNAs (Oko et al., 2019). This analysis focused on two
193 RNAs which we previously reported showed heterogeneous expression during MHV68
194 infection (Oko et al., 2019): i) ORF18, a viral RNA transcribed with late kinetics and ii) Actb, a
195 host RNA encoding beta-actin that is known to be targeted for degradation by the MHV68 SOX
196 endonuclease (Covarrubias et al., 2009).
197 As expected, mock-infected cells had no vRCA expression and a low frequency of
198 pH2AX+ events (Figure 3A). In contrast, MHV68-infected 3T12 cultures exhibited multiple
199 populations, including: 1) pH2AX- vRCA- cells (population 1, gray box, Figure 3A bottom
200 panel), 2) pH2AX+ vRCA- cells (population 2, light blue box), 3) pH2AX- vRCA+ cells
201 (population 3, orange box), and 4) pH2AX+ vRCA+ cells (population 4, red box). As these
202 studies did not use purified LANA+ cells, in contrast to the CyTOF studies, the presence of
203 these four populations suggests that these cultures contained a mixture of infected and
204 uninfected cells.
205 We next queried RNA expression within cells subdivided by pH2AX and vRCA
206 expression, using ORF18 expression as a direct readout of virus infection and Actb
207 degradation as a secondary readout of virus infection. Cells with a pH2AX- vRCA- phenotype
208 (gray box, Figure 3A-B) were present in mock- and MHV68-infected cultures, with the vast
209 majority of cells characterized by an ORF18- Actb+ phenotype and no evidence of infection
210 (Figure 3B-C). In contrast, cells with a pH2AX+ vRCA- phenotype (light blue box, Figure 3A-B)

contained ~1/3 of cells that were ORF18+ with variable expression of Actb (Figure 3B-C), identifying infection based on viral RNA expression in the absence of a viral protein. Cells with a pH2AX- vRCA+ phenotype (orange box, Figure 3A-B) were dominated by ORF18+ Actb- and ORF18- Actb- cells, demonstrating direct measures of infection by RNA and protein. Lastly, pH2AX+ vRCA+ cells (red box, Figure 3A-B) were predominantly ORF18+ Actb-, identifying viral RNA and viral protein expression in the context of host RNA degradation. These data demonstrate that pH2AX+ vRCA+ cells show progressive infection at the RNA and protein level, whereas cells expressing only vRCA or pH2AX represent intermediate infection phenotypes as measured by viral RNA expression and host RNA degradation.

scRNA-seq reveals wide variation in the frequency and magnitude of viral RNA expression

We next sought to obtain a global perspective on how MHV68 infection affects gene expression using scRNA-seq. 3T12 fibroblasts were infected with an MOI of 0.5 PFU/cell using two viruses with indistinguishable lytic replication [WT MHV68.LANAβlac and a viral cyclin-deficient (cycKO) MHV68.LANAβlac (van Dyk et al., 2000)], with LANA+ cells sort purified at 16 hpi (Figure 1A). LANA+ cells were submitted for bulk RNA-seq and scRNA-seq analysis, with a mean of 94,810 reads per cell for scRNA-seq (Figure S3A-C). While there was some concordance between the most abundant host RNAs observed in bulk RNA-seq and scRNA-seq, scRNA-seq analysis revealed wide variability among cells, a level of complexity obscured in bulk RNA-seq analysis (Figure S3D). We next focused on scRNA-seq, given its capacity to define intercellular variation and to avoid averaging of signal intensity across a population of cells. Comparison of scRNA-seq data between WT and CycKO infected cells demonstrated a similar distribution of cells and gene expression, with only five genes with average gene expression differences greater than 2-fold (Table S1 and S2), consistent with their comparable lytic replication in vitro (van Dyk et al., 2000). Therefore, subsequent analysis integrated scRNA-seq data from LANA+ cells purified from WT and CycKO infection.

To understand MHV68 transcription at the single-cell level, we first quantified the diversity and magnitude of viral transcripts. When viral RNAs (enumerated as unique molecular identifiers, UMIs) were mapped to the MHV68 genome, 77 of the 80 annotated MHV68 ORFs were detected. M10b, M10c and M12, three viral RNAs derived from MHV68 repeat structures were the only viral RNAs not detected (Virgin et al., 1997). LANA+ cells expressed a wide range of viral genes (12-66 viral genes) per cell, with a median of 52 viral genes per cell, based on detection of ≥ 1 UMI per viral gene per cell (Figure 4A). Mean UMI per viral gene and percentage of cells expressing viral genes were positively correlated (Spearman r coefficient = 0.9775), with 86.2% of LANA+ cells expressing the ORF73 RNA (Figure 4B). Despite cell purification based on uniform LANA expression, total viral UMIs per cell spanned a >1000-fold range (19-24,718 viral UMIs per cell) (Figure 4C). While the number of viral genes detected per cell was positively correlated with total viral UMIs per cell, LANA+ cells exhibited a bimodal distribution of virus RNA^{high} (Virus^{high}) cells (>500 viral UMIs/cell) and virus RNA^{low} (Virus^{low}) cells (<500 viral UMIs/cell) (Figure 4C-D). The distinction between Virus^{high} and Virus^{low} cells was not simply explained by how many viral genes were detected per cell, as some cells expressed the same number of viral genes yet showed a >10-fold variance in total viral UMIs (e.g. the range of viral UMIs among cells that express 40 viral genes per cell, Figure 4D).

To better understand viral transcription at the single-cell level, we quantified the percentage of cells expressing each viral gene (Figure 4E) and mean UMI count within positive cells (Figure 4F). The percentage of cells which expressed viral genes varied widely, with 9 viral genes (M3, ORF7, ORF17, ORF38, ORF45, ORF52, ORF58, M9, and ORF66) expressed in the vast majority (98.63-100%) of cells (Figure 4E). These ubiquitous viral RNAs spanned transcriptional categories [IE (ORF38), Early-Late (M3, ORF7), and L genes (ORF17, ORF45, ORF52, ORF58, M9, ORF66)] and kinetic classes [class I (ORF38), class II (M3, ORF45, ORF52, ORF58), class III (ORF17, M9, ORF66) and class IV (ORF7)] (Cheng et al., 2012). In

contrast, many viral genes were only detected in a subset of cells, including ORF50, an IE gene that encodes Rta, a major transcriptional regulator of lytic replication (Figure 4E). The range of expression for individual genes varied widely (Figure 4F). While many viral genes had a mean UMI per viral gene between 1-10 UMIs per cell, the most highly expressed viral gene ORF52 had a mean of >1000 UMIs per cell.

Visualization of genome-wide viral gene expression at the single-cell level

To investigate the complexity of gene expression across MHV68-infected cells, we next visualized the absolute UMI count for each viral gene across all 1,605 LANA+ cells. Cells were rank-ordered based on total viral UMIs detected per cell, from Virus^{low} to Virus^{high} cells across a 1000-fold range of viral UMIs per cell, with each row depicting expression for each MHV68 viral gene and each column depicting data from a single cell (Figure 5). This continuum of gene expression revealed multiple patterns of gene expression. First, there were some viral genes (e.g. ORF59 and ORF73βlac, which encodes LANA) which were detected in almost all cells, with only modest differences in expression between cells with the fewest viral UMIs and the greatest viral UMIs (Figure 5). Second, viral genes such as M3 and ORF52 progressively increased in expression, proportional to the increase in viral UMIs (Figure 5). Third, viral genes, including ORF48, ORF54, and ORF57, showed maximal expression in cells with intermediate viral counts (Figure 5). By stratifying cells into either Virus^{high} or Virus^{low} categories (a bifurcation identified in Figure 4C-D), we identified a subset of genes including K3, ORF42 and ORF44 whose expression was sporadic in Virus^{low} cells and uniform in Virus^{high} cells (Figure 5 and Figure S4). ORF68 was one of the only genes whose expression was slightly higher among Virus^{low} cells compared to Virus^{high} cells (Figure 5 and Figure S4). Gene expression signatures for Virus^{low} and Virus^{high} cells did not clearly track with any transcriptional or kinetic class, and individual genes within these distinctions demonstrated

288 significant gene to gene variation (Figure S5A). These data identify the highly variable nature
289 of MHV68 transcription between individual cells during de novo infection.
290
291 *MHV68-infected cells can be stratified by differential abundance of virus and host RNAs*
292 To clarify the patterns of gene expression that we observed, we used unsupervised K-
293 means clustering to identify related cells. By clustering on viral and cellular RNA expression,
294 we identified 5 clusters among LANA+ cells (Figure 6A). 3-dimensional tSNE-based data
295 visualization further identified that an IE gene (ORF50) had maximal expression in clusters A
296 and B, an early-late (E-L) gene (ORF47) had maximal expression in clusters B and C, and a L
297 gene (M7) had maximal expression in clusters D and E (Figure 6B and Figure S5B). In
298 contrast, host Actb RNA, a target of virus-induced host shutoff mediated by the ORF37 gene,
299 showed maximal expression in clusters A and B, with low expression across clusters C
300 through E (Figure 6B-C). These data suggested that at this timepoint, LANA+ cells had
301 heterogeneous virus-induced host shutoff. Cells with a high percentage of viral UMIs were
302 predominant in clusters C through E, in contrast to cells with a high frequency of host UMIs
303 prevalent in clusters A and B (Figure 6D). Based on these distinctions, we divided cells into
304 virus-based and host-biased groups (Figure 6E-F).
305 The different proportions of viral and host UMIs between virus- and host-biased cells
306 could result from changes in either how many viral or host genes were expressed, or mean
307 expression per gene. Notably, the number of virus genes expressed (defined by mean UMI per
308 cell ≥ 1) was comparable between virus-biased and host-biased cells (Figure 6G). In contrast,
309 virus-biased cells were characterized by a pronounced decrease in the number of host RNAs
310 expressed, compared to host-biased cells (Figure 6H). When we analyzed gene expression
311 levels, virus-biased cells had increased viral gene expression per cell compared to host-biased
312 cells, with no significant difference in host gene expression among expressed genes (Figure
313 6I). These data indicate that virus-biased cells have increased viral gene expression, coupled

with a pronounced reduction in the number of detectable host RNAs. While cell cycle-associated gene signatures were relatively comparable between virus-biased and host-biased cells, host-biased cells expressed a number of interferon-response genes (Figure S6 and Table S3), suggesting a potential role in resistance to infection.

Although stages of virus infection are typically defined by viral parameters only, the observations of: i) Virus^{high} and Virus^{low} cells (Figure 4D), and ii) Virus-biased and host-biased cells (Figure 6G), suggested that these two processes may be connected. Indeed, when we analyzed the distribution of cells based on the sum of all host UMIs versus the sum of all viral UMIs, we found three prominent populations (Figure 6J-K): 1) 72.8% of cells had high viral RNA expression with reduced host RNA expression (i.e. Virus^{high} Host^{low}, in red, Figure 6K), 2) 11.1% of cells had a Virus^{high} Host^{high} phenotype (in orange, Figure 6K), and 3) 14.4% of cells had a Virus^{low} Host^{high} phenotype (in blue, Figure 6K). The number of Virus^{low} Host^{high} cells almost completely corresponded with the number of Virus^{low} events which we previously identified (Figure 4D), with less than two percent of cells expressing a Virus^{low} Host^{low} phenotype (Figure 6J). By comparing viral gene expression across these 3 populations, we found that an IE gene (ORF50) and E-L gene (ORF47) had peak expression in Virus^{high} Host^{high} cells, intermediate expression in Virus^{high} Host^{low} cells, with limited expression in Virus^{low} Host^{high} cells (Figure 6L-M). In contrast, a L gene (M7) had high expression exclusively in Virus^{high} Host^{low} cells (Figure 6N). Virus^{low} Host^{high} cells had lower expression across many virus genes, with the exception of ORF68 which was modestly higher in Virus^{low} Host^{high} cells compared to other cells (Figure 6O). Actb, a known target of virus-induced shutoff, retained high expression in both Virus^{low} Host^{high} and Virus^{high} Host^{high} cells with a pronounced decrease in Virus^{high} Host^{low} cells (Figure 6P). These data demonstrate that while many LANA+ cells show signs of robust viral RNA expression coupled with reduced host RNAs, subsets of LANA+ cells express high levels of host RNAs with differential viral RNA abundance.

Correlation analysis reveals positive and negative correlations in MHV68 transcription at the single-cell level.

Finally, we sought to investigate the inter-relationships between viral genes, leveraging the unique insights obtained from single-cell data. Initially, we generated a correlation matrix of all viral gene-gene expression relationships querying all LANA+ cells. This correlation matrix identified that the majority of gene-gene pairs had a positive correlation (83.6%, depicted in blue), with fewer negative correlations (16.1%, depicted in red) (Figure S7). We next examined gene-gene relationships in Virus^{high} or Virus^{low} cells. While the majority of gene-gene relationships in Virus^{high} and Virus^{low} cells were positive correlations, Virus^{high} cells revealed an increased frequency of negative correlations (29.1%) among a subset of viral genes (Figure 7A and S7).

We next sought to investigate gene-gene relationships as of function of Virus^{high} or Virus^{low} cells. On the one hand, there were some gene pairs whose relationship was preserved between Virus^{high} and Virus^{low} cells, exemplified by ORF50 and ORF57, and ORF54 and ORF57, both showing positive correlations across Virus^{high} and Virus^{low} cells (Figure 7B-C). On the other hand, there were other gene pairs whose relationship was distinct between Virus^{high} and Virus^{low} cells. These included ORF50 and M9, and ORF54 and ORF64, with minimal correlation across total cells, a negative correlation in Virus^{high} cells, and minimal correlation among Virus^{low} cells (Figure 7B). The complexity of gene-gene expression relationships was clearly demonstrated by plotting gene-by-gene expression levels from total cells (Figure 7C-D). Predicted correlations were exemplified by a positive correlation between host RNAs Actb and Gapdh and a negative correlation between Actb and ORF64 (Figure 7C-D). While positive correlations between ORF50 and ORF57, and ORF57 and ORF54 were consistent across all events, the relationships between ORF50 and M9, ORF64 and ORF54 were more complex (Figure 7D). These data emphasize that gene-gene coexpression relationships can be

365 obscured by combining cell subsets, and emphasize the value of single-cell approaches to

366 define gene expression inter-relationships within homogeneous cell populations.

DISCUSSION

In this manuscript, we present a strategy to investigate viral infection, simultaneously quantifying viral and host RNA and protein expression in individual cells. This approach provides a conceptual framework to understand how individual cells respond to virus infection at the protein and RNA level, presents new insights into the complexity of virus infection from virus and host perspective, and establishes high-dimensional datasets as a resource for further analysis of virus-host interactions at the single-cell level. By focusing on a well-characterized virus, tightly controlled infection conditions, and cells with uniform viral gene expression, these studies emphasize the knowable complexity of infection in individual cells and the limitations of studying infection in bulk cell populations.

Implications

Our studies illustrate the power of defining virus infection by quantifying viral and host gene expression across individual cells and have significant implications for understanding virus-host interactions. First, our data highlight that gene expression analysis in a population of cells conceals wide variance in virus infection, specifically failing to identify cells with low gene expression and obscuring negative feedback mechanisms. Second, our data emphasize that defining virus infection strictly by viral gene expression ignores the essential contribution of the host cell to this process, and that virus infection stage may be more appropriately considered as the integrated impact of virus on the host. Quantitation of host RNAs and virus-dependent post-translational host modifications were particularly informative in discriminating between infection subtypes, while measures of protein abundance were less impactful. Third, our data suggest that phenotypic variation between cells, or input virions, results in cell subsets with restricted viral gene expression, a potentially novel strategy to identify negative regulators of infection. While the relative contribution of host and virus variation to these diverse outcomes

393 remains to be addressed, there is an increasing breadth of literature in support of phenotypic
394 variation from both sides (e.g. (Avraham et al., 2015; Chaturvedi et al., 2020; Hansen et al.,
395 2018; Shaffer et al., 2017)). We propose that integrated single-cell analysis of virus and host
396 will be particularly informative to understand how viral and host genes regulate infection,
397 whether influencing viral or host gene expression, and/or altering the relative proportion of
398 permissive or resistant cells. Fourth, these studies provide an opportunity to reassess
399 fundamental concepts in virology, including how variation in virus (e.g. differing ratios in
400 particle:PFU ratio (Van Skike et al., 2018)) or the host cell integrate to impact infection
401 outcome. We anticipate that further studies, combined with further mining of these datasets by
402 the community, will identify new rules governing virus infection that may be pharmacologically
403 targeted.
404
405 *Insights into herpesvirus infection*
406 Herpesvirus infection is classically divided into lytic infection, that generates new
407 infectious virions, and latent infection, that facilitates long-term persistence in host cells while
408 avoiding immune detection. Lytic infection is frequently understood as a coordinated cascade
409 of gene expression, characterized by genome-wide transcription (Pellett and Roizman, 2013).
410 High resolution mapping of coding and non-coding viral RNAs (Cheng et al., 2012; O'Grady et
411 al., 2019) and new molecular insights into the regulation of viral RNA transcription and
412 abundance (Hartenian et al., 2020) have further refined models of lytic gene expression.
413 Despite these advances, most studies have analyzed bulk cell populations, obscuring
414 intercellular heterogeneity.
415 Here, we provide three new datasets, with two complementary high-dimensional single-
416 cell approaches, CyTOF and scRNAseq, to investigate *de novo* γHV infection of cells that are
417 highly permissive for lytic infection. These studies build on our recent analysis of MHV68 gene
418 expression during *de novo* infection, studies that revealed asynchronous or inefficient infection

among MHV68-exposed cells (Oko et al., 2019). Here, we extended these studies, purifying actively-infected cells (defined by expression of the viral protein LANA, which is expressed during lytic and latent infection) and deeply characterizing RNA and protein expression profiles during *de novo* infection. By monitoring viral and host RNAs and proteins, these studies defined robust markers of productive lytic infection and revealed heterogeneity in progression following *de novo* infection.

These studies initially focused on how MHV68 infection influences cellular responses at the protein level using CyTOF. By comparing cells with or without signs of active infection, we found multiple infection phenotypes. First, LANA+ cells contained a prominent cell fraction that co-expressed high levels of a viral protein, vRCA, and phosphorylation of histone H2AX, a virus-dependent event. vRCA^{high} pH2AX^{high} cells were only found in LANA+ cells, and were further characterized by increased phosphorylation of host proteins (pRb, active β-catenin, pERK1/2, pStat1 and pAKT) consistent with reports of γHV-induced modulation of the host proteome (Chang et al., 2016). vRCA^{high} pH2AX^{high} cells also had a prominent RNA phenotype, ORF18^{high} (late viral RNA) and Actb^{low} (host RNA indicator of virus-induced host shutoff). While vRCA^{high} pH2AX^{high} ORF18 RNA^{high} Actb RNA^{low} cells showed the most progressive signs of infection, we readily identified additional cell subsets expressing viral RNA in the absence of viral protein or host-shutoff, potentially reflecting delayed infection or a disconnect between transcription and translation. These studies identify vRCA and pH2AX as strong indicators of robust and progressive virus infection, and indicate that including additional viral and host indicators can distinguish among diverse infection stages.

We next turned to scRNA-seq to gain a broader understanding of virus and host RNA expression during *de novo* infection. Though we anticipated that many LANA+ cells (i.e. vRCA^{high} pH2AX^{high} cells) would express high viral RNAs and low host RNAs (exemplified by ORF18 and Actb, respectively), the relative homogeneity of LANA+ cells at the RNA level was unknown. One of the most striking outcomes of these studies was the wide range of viral and

host gene expression observed at the single-cell level, derived from infection with a low MOI, and harvested at a single timepoint. LANA+ cells had a 1000-fold variance in total viral reads per cell, with cells expressing between 12-66 viral genes per cell and widespread variance in both the frequency and expression level of viral RNAs. While this analysis mapped RNAs to 77 of the 80 annotated MHV68 ORFs (Virgin et al., 1997) using a 3' based sequencing platform, it is notable that: i) only one viral gene (ORF52) was detected in 100% of LANA+ cells, with ii) only 9 viral genes (M3, ORF7, ORF17, ORF38, ORF45, ORF52, ORF58, M9, and ORF66) expressed in a high percentage (>98.5%) of LANA+ cells. Though many of these genes were highly expressed on a per cell basis, a high frequency of expression does not solely track with high expression. For example, ORF73 RNA, which encodes for LANA, was detected in 86.2% of cells with an average of 5 UMIs per cell. Lack of detection of ORF73 in LANA+ sort purified cells may seem to be a paradox, as cells were purified based on LANA+ cells. This apparent discordance may either be due to RNA dropout or to cells expressing LANA protein in the absence of ORF73 RNA. For other genes, limited detection likely reflects extremely low expression during lytic infection [e.g. M2, a latency-associated gene that has not historically been detected during lytic infection (Rochford et al., 2001; Virgin et al., 1999)]. These results suggest that lack of detection of some MHV68 genes is likely due to little to no expression during lytic infection and not due to technical issues with scRNA-seq. More broadly, these studies indicate that stratifying gene expression by the IE→E→L paradigm, or by kinetic class, is insufficient to describe the complexity of viral transcription in individual cells, even in a highly permissive cell type.

An important complementary perspective on virus infection was our capacity to assess how MHV68 infection remodels host RNA expression. Virus-biased cells expressed 1.5 times more viral UMIs than host UMIs, a striking result when considering that there are only 80 annotated viral ORFs (Virgin et al., 1997) compared to ~25,000 host genes (Guenet, 2005). Virus:host RNA skewing was further driven by a dramatic reduction in host gene expression,

consistent with virus-induced host shutoff (Covarrubias et al., 2011). Host shutoff was readily visualized by pronounced reduction in ActB RNA expression in vRCA^{high} pH2AX^{high} cells, illustrating the value of monitoring host RNAs at the single-cell level as an indicator of virus infection. When we assessed the global relationship between virus and host RNAs, we found additional complexity. While most LANA+ cells (73%) showed a reciprocal relationship expression of high viral RNAs and low host RNAs (i.e. Virus^{high} Host^{low}), there were substantial cell fractions that were either Host^{high}Virus^{high} or Virus^{low} Host^{high}, suggesting delayed or impaired virus-induced host shutoff (a process that requires transcription, translation and nuclease-dependent degradation of RNAs (Covarrubias et al., 2011)).

Potential relationships of virus infection phenotypes

The identification of distinct infection phenotypes raises the question of how these subsets are inter-related. Though definitive lineage relationships require sequential tracking of individual infected cells, we postulate that the Virus^{high} Host^{high} phenotype identifies cells with slower progression through lytic infection, preceding Virus^{high} Host^{low} cells. In contrast, we speculate that Virus^{low} Host^{high} cells may represent a distinct biological outcome. Although Virus^{low} cells expressed fewer viral genes, frequently at a lower magnitude, these cells contained viral RNAs from all phases of infection, with 90% of Virus^{low} cells expressing IE (ORF38), E or E-L (M3, ORF7, ORF68) or L (ORF17, ORF45, ORF52, ORF58, M9, ORF66) genes; these genes span kinetic classes, indicating that there is not a specific block in infection (Cheng et al., 2012). Virus^{low} cells did contain a few viral genes (e.g. ORF68) that are modestly increased relative to Virus^{high} cells; nonetheless, the Virus^{low} gene signature would be obscured in bulk cell analysis. The molecular basis of the Virus^{low} Host^{high} phenotype remains to be determined but could arise from host or virus variation. Curiously, Virus^{low} cells expressed multiple interferon-stimulated genes, but not type I interferons, suggesting a potential cell-intrinsic block to lytic infection. The Virus^{low} Host^{high} phenotype may also arise

497 from virus-intrinsic differences (e.g. variation in particle:PFU differences (Klasse, 2015) or
498 virus-like vesicles (Gong et al., 2017)). Variable outcomes of γHV infection have been reported
499 in multiple contexts. MHV68 infection of endothelial cells results in a significant cell fraction of
500 cells undergoing persistent infection (Suarez and van Dyk, 2008). KSHV infection of fibroblasts
501 results in variable lytic or latent infection (Jang et al., 2016; Krishnan et al., 2004; Matthews et
502 al., 2011), and EBV infection in gastric epithelial cells includes both lytic and latent outcomes
503 (Hill et al., 2013; Ma et al., 2011; Nawandar et al., 2015). Despite the restricted gene
504 expression of Virus^{low} cells, expression of multiple viral genes strongly suggests that these
505 cells have the potential to impact biological outcomes and immune regulation.
506
507 *Virus gene-gene relationships revealed by scRNA-seq*
508 Virus infection involves the coordination of highly complex gene expression patterns, a
509 poorly understand process at the single-cell level. Given this knowledge gap, we leveraged the
510 unique insights of scRNA-seq to quantify genome-wide correlation matrices. Unexpectedly, we
511 found gene pairs which were differentially regulated between Virus^{high} or Virus^{low} subsets,
512 including pronounced negative correlations among Virus^{high} cells. The complexity of these
513 relationships was illustrated by examining correlations between ORF50 and other viral genes.
514 ORF50 encodes the Rta viral transactivator and is known to both induce and repress
515 transcriptional targets (Coleman et al., 2005; Damania et al., 2004; Hair et al., 2007; Pavlova
516 et al., 2005; Wu et al., 2000). Correlation analysis among Virus^{high} cells corroborated
517 established ORF50 targets (e.g. positive correlation with ORF57, negative correlation with
518 ORF73) and identified new potential relationships (e.g. positive correlation with ORF54 and M8
519 and negative correlation with ORF64-67). These findings emphasize the importance of defining
520 gene expression relationships in biologically homogeneous populations, something uniquely
521 afforded by single-cell analysis.

Our scRNA-seq analysis quantified viral RNA abundance in LANA+ cells, mapping RNAs to the annotated MHV68 genome using polyA-primed sequencing. This resource illustrates the complexity of viral RNA expression following *de novo* γHV infection and sets the foundation for new insights in gene expression in individual cells, including how virion-packaged RNAs shape expression, the relative contribution of transcription and RNA decay to the transcriptome, and RNA:protein relationships in individual cells (Hartenian and Glaunsinger, 2019; Purushothaman et al., 2015; Ruiz et al., 2019). This approach further emphasizes that not all abundant viral RNAs are equally expressed at the single-cell level, and argue for the importance of single-cell analysis to identify candidate immunogens based on uniform, high expression.

In total, these studies provide a resource to understand the complexity of virus-host interactions within individual cells. This work provides three databases from matched *de novo* gammaherpesvirus infection of a single permissive cell type, from CyTOF to bulk RNA-seq to scRNA-seq, and exemplify the power of these approaches to reveal new insights into virus-host interaction during γHV infection. We anticipate that these data will serve as an important benchmark for future studies of virus infection, providing a wealth of observations to further revise our understanding of virus-host interactions.

ACKNOWLEDGEMENTS

The authors would like to acknowledge insightful comments made by the members of the Clambey and van Dyk laboratories, and the laboratories of Dr. Kelly Doran and Dr. Laurel Lenz for equipment and reagents. We acknowledge flow cytometry support through ClinImmune and the Department of Immunology & Microbiology, CyTOF services through the Flow Cytometry Shared Resource (FCSR) of the University of Colorado Cancer Center (UCCC), expert technical assistance regarding CyTOF from Christine Childs and Karen Helm, receipt of CyTOF antibodies through the coordinated efforts of the FCSR and the Human Immune Monitoring Shared Resource, and support of sequencing through the Genomics Shared Resource of the UCCC.

FUNDING

This research was funded by National Institutes of Health grants R01CA103632 and R01CA168558 to L.F.V.D., R21AI134084 to E.T.C. and L.F.V.D., T32AI052066 to J.L.B., and Colorado CTSI Novel Methods grant to E.T.C.. The Colorado CTSI is supported by NIH/NCATS Colorado CTSA Grant Number UL1 TR002535. The Flow Cytometry, Genomics, and Human Immune Monitoring Shared Resources of the University of Colorado Cancer Center receive direct funding support from the National Cancer Institute through Cancer Center Support Grant P30CA046934. Contents are the authors' sole responsibility and do not necessarily represent official NIH views. The funders had no role in study design, data collection and analysis, decision to publish, or preparation of the manuscript.

DECLARATION OF INTERESTS

The authors declare no competing interests.

AUTHOR CONTRIBUTIONS

Conceptualization: Jennifer N. Berger, Brian F. Niemeyer, Eric T. Clambey, Linda F. van Dyk

Data curation: Bridget Sanford, Abigail K. Kimball, Kenneth L. Jones, Eric T. Clambey

Formal analysis: Jennifer N. Berger, Bridget Sanford, Abigail K. Kimball, Kenneth L. Jones, Eric T. Clambey

Funding acquisition: Eric T. Clambey, Linda F. van Dyk

Investigation: Jennifer N. Berger, Lauren M. Oko, Rachael E. Kaspar, Brian F. Niemeyer

Methodology: Jennifer N. Berger, Bridget Sanford, Lauren M. Oko, Abigail K. Kimball, Rachael E. Kaspar, Brian F. Niemeyer, Kenneth L. Jones

Project administration: Eric T. Clambey, Linda F. van Dyk

Resources: Jennifer N. Berger, Bridget Sanford, Abigail K. Kimball, Kenneth L. Jones, Eric T. Clambey, Linda F. van Dyk

Software: Abigail K. Kimball, Eric T. Clambey, Bridget Sanford, Kenneth L. Jones

Supervision: Eric T. Clambey, Linda F. van Dyk

Validation: Jennifer N. Berger, Bridget Sanford, Abigail K. Kimball, Eric T. Clambey, Linda F. van Dyk

Visualization: Jennifer N. Berger, Bridget Sanford, Abigail K. Kimball, Kenneth L. Jones, Eric T. Clambey, Linda F. van Dyk

Writing – original draft: Jennifer N. Berger, Eric T. Clambey, Linda F. van Dyk

Writing – review & editing:

583 **FIGURE LEGENDS**

584

585 **Figure 1. CyTOF analysis identifies a distinct protein expression profile for virally-**
586 **infected cells.** High-dimensional single-cell protein analysis of MHV68 infection by CyTOF. (A)
587 3T12 fibroblasts were either mock or MHV68-infected with WT MHV68.LANAβlac (MOI=0.5),
588 with indicated populations FACS purified according to LANA::β-lactamase expression at 16
589 hours pi. (B) PhenoGraph analysis of mock, LANA- and LANA+ cells subjected to CyTOF
590 analysis and visualized by tSNE-based dimensionality reduction identified 14 cell clusters
591 (colored by cluster ID). (C) Comparison of the frequency (left) and protein expression profile
592 (right) of PhenoGraph-defined clusters in LANA- and LANA+ samples. Clusters (in rows),
593 ranked from those exclusively in LANA- samples (top) to those exclusively in LANA+ samples
594 (bottom); asterisks indicate clusters statistically significantly different between conditions,
595 defined by unpaired t-test corrected for multiple comparisons using the Holm-Sidak method,
596 $p<0.05$. Data show mean ± SEM with individual symbols indicating individual sample values
597 (n=4 per group). Relative protein expression for each cluster (right panel) is indicated by
598 heatmap intensity, with protein markers divded by functional categories. (D) tSNE plot of
599 LANA- and LANA+ cells colored according to LANA- and LANA+ exclusivity (left), vRCA
600 expression (middle), and pH2AX expression (right panel). Red and blue lines identify events
601 exclusive to LANA+ or LANA- clusters (left panel). Ruler defines range of expression with
602 values calculated using the equation arcsinh (x/5) where x is raw expression value. Live, DNA+
603 cells (^{191}Ir+ ^{193}Ir+ ^{195}Pt-) were imported into PhenoGraph with 9,162 events total analyzed
604 (1,018 events from each sample; n=1, mock, n=4 each for LANA+ and LANA- samples),
605 clustered on 9 cell surface proteins (vRCA, BST2, CD9, CD29, CD44, CD63, Ly6A/E, Ly6C,
606 and MHCI). See also Figure S1.

607

608 **Figure 2. LANA+ cells show heterogeneous protein and post-translational modifications**
609 **during lytic infection.** CyTOF analysis of LANA+ MHV68-infected cells as in Figure 1. (A)
610 PhenoGraph analysis of 40,000 LANA+ cells (10,000 cells/sample, 4 samples) clustered by 9
611 cell surface proteins (vRCA, BST2, CD9, CD29, CD44, CD63, Ly6A/E, Ly6C, and MHCI)
612 identified 15 unique cellular clusters colored by cluster ID and displayed on a tSNE plot. (B)
613 LANA+ cells can be stratified into six categories based on expression of pH2AX, vRCA, Ly6C,
614 and BST2, with (C) LANA+ cells colored by expression levels for each protein marker. Ruler
615 defines range of expression with values calculated using the equation arcsinh (x/5) where x is
616 raw expression value. (D) LANA+ cells were divided into $pH2AX^{Lo}$ and $pH2AX^{Hi}$ events, and
617 compared for raw median expression. Data depict proteins whose expression was statistically
618 significantly different between $pH2AX^{Lo}$ and $pH2AX^{Hi}$ events. Data depict mean ± SEM with
619 individual symbols indicating values from independent samples (n=4/group). All samples were
620 analyzed for statistical significance using unpaired t tests, corrected for multiple comparisons
621 using the Holm-Sidak method, with statistical significance denoted as *p<0.05, ** p<0.01,
622 ***p<0.001. See also Figure S2.
623
624 **Figure 3. MHV68-infected cells with a $pH2AX^{high}$ $vRCA^{high}$ cell phenotype express high**
625 **viral mRNA and low host actin RNA**. Flow cytometric analysis of protein and RNA
626 expression in 3T12 fibroblasts infected with MHV68 (MOI=0.5, harvested 16 hpi). (A) Analysis
627 of vRCA and pH2AX protein expression in mock and MHV68-infected cultures identified four
628 populations denoted by numbers and color (1=Gray, 2=Blue, 3=Orange, 4=Red). (B) Analysis
629 of viral ORF18 and host Actin (Actb) mRNA expression across four populations of MHV68-
630 infected cultures, stratified by vRCA and pH2AX expression. Border color of biaxial plots
631 corresponds to the parent population stratified by protein expression in panel A. (C)
632 Quantitaiton of the frequency of cells based on RNA expression profile as in panel B, depicting

633 mean ± SEM from 3 independent experimental samples. Flow cytometric analysis was done
634 on singlets, following gating to remove doublets.
635
636 **Figure 4. scRNA-seq reveals wide variation in the frequency and magnitude of viral RNA**
637 **expression.** scRNA-seq analysis of MHV68 viral gene expression in LANA+ 3T12 fibroblasts
638 as in Figure 1A. (A) LANA+ cells show a wide range in how many viral genes are expressed on
639 a per-cell basis. Expression of a viral gene was defined conservatively as any viral gene with
640 ≥1 UMI detected per cell, with data showing the distribution of cells based on number of viral
641 genes expressed per cell. (B) Viral genes vary widely in mean UMI per cell and the frequency
642 of cells expressing an individual viral gene. Mean viral UMI per cell was calculated from
643 positive cells that expressed ≥1 UMI per gene, with five representative genes identified by
644 unique shading. Each dot represents expression for a single viral gene product for all 80
645 annotated MHV68 open reading frames. (C) The distribution of cells based on total viral UMIs
646 reveals a bimodal distribution of virus low and virus high cells. (D) Total viral UMIs per cell as a
647 function of the number of viral genes detected per cell (as in panel A). Cells demonstrate a
648 bimodal distribution of total viral UMIs with virus high and low cells, with a positive Spearman
649 correlation coefficient, rs, as indicated. (E) Frequency of cells expressing each viral gene, with
650 viral gene expression defined as ≥1 UMI for each viral gene. Dashed line indicates 50% of
651 events. (F) Mean UMI count per viral gene, defined by calculating mean value only from
652 positive cells (≥1 UMI for each viral gene), depicting mean ± SD. Data represent scRNA-seq
653 data from all LANA+ cells (n=1605 cells). nd, genes that were not detected. See also Figure
654 S3 and Table S1.
655
656 **Figure 5. Visualization of genome-wide viral gene expression at the single-cell level.**
657 scRNA-seq analysis of MHV68 gene expression in LANA+ 3T12 fibroblasts as depicted in
658 Figure 1A. Comprehensive visualization of viral gene expression on a single cell basis. Each

659 row depicts expression pattern for a different viral gene. Each column depicts expression
660 within an individual cell. Cells are rank ordered from the cell with the least (left) to the greatest
661 total viral UMI count (right), with corresponding total viral (filled orange line) and host (black
662 dots) UMIs per cell depicted in the bottom panel. Cells are further bisected into Virus low cells
663 (< 500 viral UMIs per cell) and Virus high cells (> 500 viral UMIs per cell) by a thick vertical
664 black line, from a total of 1605 cells. UMI counts are stratified based on the indicated heatmap
665 scale. See also Figure S4.

666

667 **Figure 6: MHV68-infected cells can be stratified by differential abundance of virus and**
668 **host RNAs.** scRNA-seq analysis of MHV68-infected LANA+ cells for viral and host RNAs. (A-
669 E) 3D tSNE-based dimensionality reduction was used to visualize gene expression within
670 individual cells. (A) K-means clustering identified 5 unique cell clusters, as labelled. (B) Viral
671 and host RNAs show different patterns of expression, comparing viral immediate early (IE),
672 early-late (E-L) and late (L) genes with host beta actin (Actb). UMI counts visualized in
673 individual cells (symbols) as defined by key. (C) The ratio of host Actb to ORF37 UMIs,
674 calculated for each cell and overlaid onto tSNE-based visualization, varies widely across cells.
675 (D) Percent of viral (left) and host UMIs (right) per cell was calculated for each cell, portrayed
676 by shade of color overlaid onto tSNE visualization. (E) Cells were separated into two groups:
677 virus biased (red) and host biased (black) based on percent viral and host UMIs, and K-means
678 clustering. Host biased cells included clusters A and B with <20% virus UMIs on a per cell
679 basis. (F) Characteristics of virus and host biased cells based on scRNA-seq data. (G-H)
680 Number of (G) viral or (H) host genes with mean UMI expression $\geq$1, among either virus (open
681 red symbol) or host biased cells (dashed black line). (I) Violin plots depict the distribution of
682 mean gene expression among expressed genes (mean UMI expression $\geq$1), comparing viral
683 genes (left) or host genes (right) in either virus biased (open red symbol) or host biased cells
684 (open black line). Quartiles and median are depicted in each violin plot. Statistical comparisons

compared viral or host genes and their difference between virus and host biased cells. ****p<0.0001, one way ANOVA with Tukey's multiple comparisons test. ns, not significant. (J-K) Biaxial analysis of LANA+ cells (n=1605 cells) comparing total host UMI count (y axis) versus total viral UMI count (x axis) identified three major cell populations, stratified by differential expression of viral or host genes. (K) Identification of cells that are Virus^{low} Host^{high} (blue), Virus^{high} Host^{high} (orange), and Virus^{high} Host^{low} (red). (L-P) Histogram overlays comparing relative expression of (L-O) viral and (P) host genes for the three identified cell populations. Each gene is denoted by its IE, E, or L class and by its kinetic class defined by (Cheng et al., 2012). See also Figure S5-6, Table S2.

Figure 7. Correlation analysis reveals positive and negative correlations in MHV68 transcription at the single-cell level. The inter-relationship of viral gene expression was interrogated using scRNA-seq data from MHV68-infected LANA+ cells. (A) Correlation matrix of viral genes among Virus^{high} cells (>500 viral UMIs/cell), depicting Spearman correlation coefficient, rs, for each gene pair according to the indicated heatmap. Positive correlation is indicated by blue, negative correlation indicated by red. Correlation matrix depicts all viral genes except for M10b and M10c (X indicates gene for which there were no values) and M12, M13 and M14 (excluded due to negligible values). (B) A comparison of correlation coefficients between viral gene pairs when analyzing all cells (top), Virus^{high} (middle) or Virus^{low} (bottom) cells. Data identify discrepant correlations observed in different cell subsets. (C) Examples of host and virus gene pairs with positive correlations, demonstrated by plotting scRNA-seq gene expression values on biaxial plots across all LANA+ cells. (D) Examples of host and virus gene pairs with a lack of correlation or negative correlation. Panels in C-D depict scRNA-seq values for all LANA+ cells (n=1,605 cells), including both Virus^{high} and Virus^{low} events. Each plot includes the Spearman correlation coefficient for the indicated gene pair defined across all cells. See also Figure S7.

STAR ★ METHODS

Contact for Reagent and Resource Sharing

Further information and requests for resources and reagents should be directed to, and will be fulfilled by, the Lead Contact, Linda van Dyk (Linda.vanDyk@cuanschutz.edu).

Experimental Model and Subject Details

Viruses

All experiments used WT MHV68 (strain WUMS; ATCC VR-1465) (Virgin et al., 1997), using either bacterial artificial chromosome–derived WT MHV68 (Adler et al., 2000) or WT MHV68.LANAβlac, which encodes a fusion between ORF73 and the beta-lactamase gene (Nealy et al., 2010). Certain studies were done using a variant engineered to contain a translational stop in the ORF72 (v-cyclin) gene, on the WT MHV68.LANAβlac background (Niemeyer et al., 2018). MHV68 was grown and titrated by plaque assay on 3T12 fibroblasts, as previously published (Diebel et al., 2015).

Cell Culture

NIH 3T12 cells (ATCC # CCL-164) were grown in Dulbecco's modified Eagle medium (DMEM, Gibco, Life Technologies) supplemented with 5% fetal bovine serum (Atlanta Biologicals), 1x Penicillin-Streptomycin-L-Glutamine (Gibco, Life Technologies). Cells were passaged using 0.05% trypsin (Gibco, Life Technologies) after washing with 1x PBS (Gibco, Life Technologies). Cells were maintained at 37^{o}C in a 5% CO_2 humidified incubator (Forma Scientific).

Method Details

RNA sequencing and Analysis

3T12 fibroblasts were infected at an MOI=0.5 with a low volume inoculum for one hour, after which inoculum was removed and cells were rinsed. Cells were harvested at 16 hours post-

infection (hpi) and stained with β-lactamase substrate as previously reported (Diebel et al., 2015) using the CCF2-AM substrate (Invitrogen, Life Technologies). Cells were subjected to fluorescence activated cell sorting (FACS), with cells gated on singlet cells that were positive for the cleaved CCF2-AM substrate. Cleavage of CCF2-AM was defined as positive fluorescence in the violet laser-excited 450nm emission channel obtained in WT MHV68.LANAβlac or cycKO MHV68.LANAβlac-infected cultures, compared to parental WT MHV68 infected cultures with no beta-lactamase fusion gene, used to define background fluorescence. β-lactamase positive cells were sorted using a FACSAria Fusion (BD Biosciences). Cells were spun down at 1,200 RPM (Sorvall RT60003), and resuspended in 1x PBS (Gibco, Life Technologies). Cells were either prepared for CyTOF or RNA-sequencing by the Genomics and Microarray Shared Resource Core at University of Colorado. Bulk RNA-seq libraries were sequenced using Illumina HiSeq4000 platform with single-end reads (1 × 151), with forty million reads per sample collected and resulting sequences filtered and trimmed to remove low-quality bases (Phred score <15), and analyzed using a custom computational pipeline consisting of open-source gSNAP, Cufflinks. Single cell RNA Sequencing (scRNA-seq) (1000 cells per sample) was submitted for single cell barcoding and cDNA synthesis on a 10x Genomics Chromium Controller (10x Genomics), with recovered cell number and sequencing depth for scRNA-seq described in Figure S3. cDNA was sequenced using the NovaSEQ 6000 instrument with an S4 Flow Cell (Illumina). Sequence data was analyzed as follows: Cellranger (2.0.2) count module was used for alignment, filtering, barcode counting and UMI counting of the single cell FASTQs. tSNE coordinates were determined by CellRanger.

PrimeFlow RNA Assay

3T12 fibroblasts were infected at an MOI=1.0 with a small-volume inoculation. Inoculum was removed and rinsed-off with PBS after one hour and growth medium was replaced. Cells were

763 harvested 16 hpi and processed for flow cytometry using the PrimeFlow RNA Assay (Thermo
764 Fisher) as described previously (Oko et al., 2019). Briefly, cells were stained with a rabbit
765 antibody against the MHV68 ORF4 protein (vRCA), labeled with a Zenon R-phycoerythrin
766 rabbit IgG label reagent (Life Technologies) per manufacturer's protocol (Oko et al., 2019).
767 Following cell fixation, cells were then subjected to fluorescent barcoding, labeling distinct
768 experimental conditions with either Ghost Dye Violet 450 (Tonbo Biosciences), Ghost Dye
769 Violet 510 (Tonbo Biosciences) or leaving the cells unlabeled. Labelled samples were then
770 combined into a single tube and subjected to probe hybridization for viral and host RNAs or
771 proteins following the manufacturer's protocol. Flow cytometric analysis was done on an LSR II
772 instrument (BD Biosciences). Compensation values were initially based on antibody-stained
773 beads (BD Biosciences) and cross-validated using cell samples stained with individual
774 antibody conjugates, with compensation modified as needed post-collection using FlowJo.
775 PrimeFlow probes and antibodies included: i) a type 6 (AlexaFluor750)-mouse actb probe, ii) a
776 type 4 (AF488)-MHV68 ORF18 probe, iii) PE-labelled anti-vRCA antibody, and iv) AF647-
777 conjugated anti-mouse phospho-histone H2AX antibody (clone JBW301, that recognizes
778 phosphorylated serine 139 of H2AX).
779
780 CyTOF Sample Preparation and Data Acquisition
781 CyTOF antibodies were obtained from Fluidigm (previously DVS Sciences), provided by the
782 University of Colorado CyTOF Antibody Bank, supported by the Flow Cytometry Shared
783 Resource and the Human Immune Monitoring Shared Resource of the University of Colorado
784 Cancer Center. Samples were FACS purified based on LANA::β-lactamase dependent CCF2-
785 AM cleavage, into either LANAβlac+ or LANAβlac- fractions, transferred to 5mL screw cap
786 tubes, spun down, and stained for viability using 5 μM Cell-ID Cisplatin (Fluidigm) diluted in 1X
787 PBS (Rockland Immunochemicals) for 5 minutes at RT. Samples were then washed, fixed, and
788 each sample labelled with a series of unique palladium isotopic barcodes (Cell-ID 20-Plex

789 Palladium (Pd) Barcoding Kit, Fluidigm). After samples were washed and pooled, cells were
790 pre-treated with 2.4G2 Fc receptor blockade (Tonbo) using a 1:100 dilution of antibody. Cells
791 were incubated with a panel of antibodies, diluted in Maxpar Cell Staining Buffer (Fluidigm), to
792 detect cell surface proteins, washed, then incubated with secondary detection antibodies (anti-
793 FITC, anti-PE, anti-APC, anti-Biotin, and goat anti-rabbit isotopically labelled antibodies)
794 (Kimball et al., 2019). Samples were washed, fixed, and permeabilized (eBioscience Foxp3 /
795 Transcription Factor Staining Buffer Set, Thermo Fisher) before incubation with antibodies to
796 intracellular proteins. The sample was washed, fixed with freshly made 1.6%
797 paraformaldehyde diluted in Maxpar PBS (16% paraformaldehyde, Alfa Aesar), incubated in
798 0.125nM Iridium intercalator diluted in Maxpar PBS (Fluidigm), and stored at 4˚C until
799 acquisition. Samples were washed with 3ml of Maxpar Cell Staining Buffer, washed two times
800 with deionized water (Milli-Q®), resuspended in deionized water (Milli-Q) containing 1:9 EQ
801 Four Element Calibration Beads (Fluidigm), filtered through CellTrics 30um disposable filters
802 (Sysmex-Partec), and counted with a BIORAD TC20 automated cell counter. Data was
803 acquired on the Helios mass cytometer (Fluidigm). To ensure an appropriate flow rate though
804 the Helios, the sample volume was adjusted with the EQ Four Element Calibration Beads
805 (Fluidigm)/deionized water (Milli-Q) to dilute the sample to 1 million cells/mL at an acquired
806 event rate of 400,000-500,000 events/hr.
807
808 CyTOF sample normalization/debarcoding
809 Data were normalized with bead-based normalization using NormalizerR2013b_MacOSX and
810 then debarcoded using SingleCellDebarcoderR2013b_ MacOSX, using software downloaded
811 from the Nolan laboratory GitHub page (https://github.com/nolanlab). Normalized and
812 debarcoded data were subjected to traditional Boolean gating in FlowJo, identifying DNA+
813 events (^{191}Iridium (Ir)+ ^{193} Ir+) that were viable (^{195} Platinum(Pt)−), exported for downstream
814 analysis in PhenoGraph.

815

816 CyTOF Data Analysis

817 Normalized and debarcoded live DNA+ events were imported into cytofkit, and subjected to the
818 PhenoGraph algorithm. Clustering was done on either 9 cell surface proteins (Figures 1-2) or
819 all 23 proteins (Figure S1) . PhenoGraph was run with the following settings: 1) Merge method:
820 “min” (Figures 1, S1) or “ceiling: 10,000 events” (Fig. 2), 2) Transformation method:
821 “cytofAsinh”, 3) Clustering method: “Rphenograph”, and 4) Visualization method: “tSNE”. All
822 other settings were selected by default. Median marker intensity for mock, LANA-, and LANA+
823 samples was calculated in FlowJo. Statistical significance was tested in GraphPad Prism
824 using an unpaired t test, with statistical significance as identified.

825

826 PhenoGraph visualization and analysis

827 PhenoGraph tSNE plots were visualized and customized in the R package “Shiny” (Kimball et
828 al., 2018). In the “Shiny” application cluster color was customized, tSNE plots were colored
829 according to the expression of various cellular markers, and dendrograms were generated.
830 The “cluster cell percentage” .csv file was used for comparing the distribution of events
831 between conditions and determining statistical significance.

832

833 RT-qPCR

834 RNA was isolated using the RNeasy Micro Kit (Qiagen) following manufacturer’s
835 specifications. DNA contamination was removed using Turbo-DNAse (ThermoFisher)
836 according to the manufacturer’s specifications. RT-qPCR for Ifnb1 was performed using a
837 primer/probe set (ThermoFisher) and the LightCycler 480 Probes Master (Roche) in 384-well
838 plates on the QuantStudio 7 Flex Instrument (Applied Biosystems, Life Technologies). RNA
839 was reverse transcribed with SuperScript II (Invitrogen) and qPCR was performed using iQ
840 SYBR Green SuperMix (Bio-Rad) in 384-well plates on the QuantStudio 7 Flex instrument

(Applied Biosystems, Life Technologies). qRT-PCR results were analyzed using the Pfaffl method, as described by (Pfaffl, 2001), with standardization relative to 18S.

Quantification and Statistical Analysis

Data from the 10X Genomics Chromium Controller (10x Genomics) were analyzed with CellRanger, including calculation of cell coordinates for 3D tSNE plots, visualized in Plotly. Unbiased K means clustering was carried out using the DoKmeans function in Seurat. SeqGeq was used for biaxial plotting of scRNAseq data. All flow cytometry data analysis was performed using FlowJo V.10.0.8r1 with flow cytometry data shown as dot plots or averaged for bar graphs. Statistical significance was tested using unpaired student's t test or one-way ANOVA analysis with Tukey's multiple comparisons test. Statistical analysis and graphing were performed with GraphPad Prism 7.0d or higher. Gene expression correlation was determined with Spearman's correlation analysis in GraphPad Prism (8.4.2). CyTOF analysis was done using PhenoGraph as described above or in (Kimball et al., 2018). p values less than 0.05 were considered significant.

Data and Software Availability

CyTOF data have been deposited to FlowRepository.org and will be made publicly available upon manuscript acceptance. RNA-Seq data have been deposited to NCBI GEO and will be made publicly available upon manuscript acceptance.

861 **Key Resources Table**

REAGENT or RESOURCE	SOURCE	IDENTIFIER
Antibodies		
Anti-beta-Catenin (clone D13A1) – 165Ho	Fluidigm	Cat#: 3165027A, RRID: AB_2811247
Anti-Human/Mouse CD44 (clone IM7) – 171Yb	Fluidigm	Cat#: 3171003B
Anti-IkBa (amino-terminal antigen) (clone L35A5) – 164Dy	Fluidigm	Cat#: 3164004A, RRID: AB_2811249
Anti-Ki67 (clone B56) – 161Dy	Fluidigm	Cat#: 3161007B, RRID: AB_2811255
Anti-Mouse Ly-6A/E (Sca-1) (clone D7) – 169Tm	Fluidigm	Cat#: 3169015B, RRID: AB_2811233
Anti-Mouse Ly-6C (clone HK1.4) – 162Dy	Fluidigm	Cat#: 3162014B
Anti-Mouse MHC Class I (clone 28-14-8) – 144Nd	Fluidigm	Cat#: 3144016B, RRID: AB_2687831
Anti-Human cleaved PARP (clone F21-852) – 143Nd	Fluidigm	Cat#: 3143011A
Anti-p-p38 [T180/Y182] (clone D3F9) – 156Gd	Fluidigm	Cat#: 3156002A, RRID: AB_2661826
Anti-p4E-BP1 [T37/T46] (clone 236B4) – 149Sm	Fluidigm	Cat#: 3149005A, RRID: AB_2847866
Anti-pAkt [S473] (clone D9E) – 152Sm	Fluidigm	Cat#: 3152005A, RRID: AB_2811246
Anti-pERK 1/2 [T202/Y204] (clone D1314.4E) – 167Er	Fluidigm	Cat#: 3167005A, RRID: AB_2661834

Anti-pHistone H2A.X [Ser139] (clone JBW301) - 147Sm	Fluidigm	Cat#: 3147016A, RRID: AB_2847865
Anti-pRb [S807/811] (clone J112-906) – 150Nd	Fluidigm	Cat#: 3150013A, RRID: AB_2811254
Anti-pS6 [S235/S236] (clone N7-548) –172Yb	Fluidigm	Cat#: 3172008A, RRID: AB_2811251
Anti-pSHP2 [Y580] (clone D66F10) – 141Pr	Fluidigm	Cat#: 3141002A, RRID: AB_2811252
Anti-pStat1 [Y701] (clone 58D6) – 153Eu	Fluidigm	Cat#: 3153003A, RRID: AB_2661824
Anti-pStat3 [Y705] (clone 4/P-Stat3) – 158Gd	Fluidigm	Cat#: 3158005A, RRID: AB_2661827
Anti-APC (clone APC003) – 176Yb	Fluidigm	Cat#: 3176007B, RRID: AB_2811236
Anti-Biotin (clone 1D4-C5) – 170Er	Fluidigm	Cat#: 3170003B, RRID: AB_2811234
Anti-FITC (clone FIT-22) – 160Gd	Fluidigm	Cat#: 3160011B, RRID: AB_2811235
Anti-PE (clone PE-001) – 145Nd	Fluidigm	Cat#: 3145006B, RRID: AB_2687631
APC anti-mouse CD137 (Bst2, PDCA-1) (clone 927)	BioLegend	Cat#: 127015, RRID: AB_1967101
Biotin anti-mouse/rat CD29 (clone HMβ1-1)	BioLegend	Cat#: 102203, RRID: AB_312880

FITC anti-mouse CD9 (clone MZ3)	BioLegend	Cat#: 124807, RRID: AB_1279324
Goat Anti-Rabbit (polyclonal) – 175Lu	Fluidigm	Cat#: 3175002G
PE anti-mouse CD63 (clone NVG-2)	BioLegend	Cat#: 143903, RRID: AB_11203532
Purified Anti-Mouse CD16/CD32 (clone 2.4G2)	Tonbo	Cat#: 70-0161-U500, RRID: AB_2621487
vRCA Ab (goat polyclonal antiserum)	Dr. H.W. Virgin IV	Laboratory generated polyclonal antiserum
Alexa Fluor 647-conjugated anti-phospho Histone H2A.X [S139] (clone JBW301)	MilliporeSigma	Cat#: 05-636-AF647
Chemicals, Peptides, and Recombinant Proteins		
Paraformaldehyde (PFA), 16% w/v aqueous solution, methanol free	Alfa Aesar by Thermo Fischer	Cat#: 43368
1x PBS	Gibco, Rockland Immunochemicals	Cat#: 10010-023
Barcoding Perm Buffer (10X)	Fluidigm	Cat#: 201057
Cell-ID™ 20-Plex Pd Barcoding Set	Fluidigm	Cat#: PN S00114
Cell-ID™ Cisplatin	Fluidigm	Cat#: 201064
Cell-ID™ Intercalator-Ir	Fluidigm	Cat#: 201192B
Water, deionized distilled	Millipore	Cat#: EM3234
DMEM, high glucose	Gibco, Life Technologies	Cat#: 11965-118

eBioscience™ Foxp3 / Transcription Factor Fixation/Permeabilization Concentrate and Diluent	Invitrogen by Thermo Fisher	Cat#: 00-5523-00
EQ™ Four Element Calibration Beads	Fluidigm	Cat#: 201078
Fetal Bovine Serum	Atlanta Biologicals	Cat#: S11550
iQ SYBR Green Supermix	Bio-Rad	Cat#: 170-8882
Lightcycler 480 Probes Master	Roche Molecular Systems	Ref#: 04707494001
Maxpar Cell Staining Buffer	Fluidigm	Cat#: 201068
Maxpar Fix I Buffer (5X)	Fluidigm	Cat#: S00115
Maxpar PBS	Fluidigm	Cat#: 201058
Penicillin-Streptomycin-Glutamate (100x)	Gibco, Life Technologies	Cat#: 10378016
Poly(I:C) HMW	Invivogen	Cat#: tlrl-pic
Proteinase K	Promega	Cat#: V3021
Sodium Chloride	ThermoFisher	Cat#: BP-358-212
SuperScript II Reverse Transcriptase	Invitrogen, Thermo Fisher	Cat#: 18064014
Trypsin-EDTA (0.05%), phenol red	Gibco, Thermo Fisher	Cat#: 25300-054
TURBO DNase (2 U/μL)	ThermoFisher	Cat#: AM2238
X-tremeGENE HP DNA transfection reagent	Sigma-Aldrich	Cat#: 6366236001
Critical Commercial Assays		

DNeasy Blood and Tissue Kit	Qiagen	Cat#: 69506
LiveBLAzer FRET-B/G Loading Kit with CCF2-AM	Life Technologies, ThermoFisher	Cat#: K1032
OneStep RT-PCR Kit	Qiagen	Cat#: 210212
PrimeFlow™ RNA Assay Kit	ThermoFisher	Cat#: 88-18005-210
RNeasy Micro Kit	Qiagen	Cat#: 74004
Zenon™ R-Phycoerythrin Rabbit IgG Labeling Kit	Invitrogen, ThermoFisher	Cat#: Z25355
Deposited Data		
Raw CyTOF data	This study	FlowRepository.org
Raw single cell RNAseq data	This study	GEO
Experimental Models: Cell Lines		
Murine 3T12 fibroblasts (BALB/3T12-3)	ATCC	ATCC CCL-164™
Experimental Models: Organisms/Strains		
Murine gammaherpesvirus 68 (Wild-type, WT MHV68)	L.F. van Dyk	(Virgin et al., 1997)
Murine gammaherpesvirus 68 with a LANA::βlac gene fusion (WT MHV68.blac)	L.F. van Dyk	(Nealy et al., 2010)
Murine gammaherpesvirus 68 cyclin-deficient virus with a LANA::βlac gene fusion (CycKO MHV68.blac)	L.F. van Dyk	(Niemeyer et al., 2018)
Oligonucleotides		
MHV68 ORF18 probe, Type 4 (AlexaFluor 488)	Thermo Fisher	VF4-60000512

Mouse Actb probe, Type 6 (AlexaFuor750)	Thermo Fisher	VB6-12823
Mouse 18S primer/probe set	Thermo Fisher	Cat#: Mm03928990_g1
Mouse 18S Quantitect Primer Assay	Qiagen	Cat#: QT00199367
Mouse Ifnb1 primer/probe set	Thermo Fisher	Cat#: Mm00439552_s1
Software and Algorithms		
Adobe Illustrator 24.1.3	Adobe	www.adobe.com/illustrator
Bead Normalization (NormalizerR2013b_MacOSX)	Github	https://github.com/nolanlab/bead-normalization
Cell Ranger	10x Genomics	https://www.10xgenomics.com
Cytofkit v3.8	Bioconductor	http://bioconductor.org/packages/release/bioc/html/cytofkit.html
FlowJo v10.4.2 and v10.6.1	FlowJo	https://www.flowjo.com
GraphPad Prism 7.0 and 8.0	GraphPad	https://www.graphpad.com
Matlab	MathWorks	https://www.mathworks.com/products/matlab.html
Microsoft Excel 15.28	Microsoft	www.microsoft.com
Microsoft Office 15.28	Microsoft	www.microsoft.com
R studio v1.1.453	R studio	https://www.rstudio.com/
SeqGeq 1.6.0	FlowJo	https://www.flowjo.com
Seurat	Satija lab	https://www.satijalab.org/seurat
Single Cell Debarcoder (SingleCellDebarcoderR2013b_ MacOSX)	Github	https://github.com/nolanlab/single-cell-debarcoder
XQuartz v2.7.11	XQuartz	https://www.xquartz.org

862

REFERENCES

Adang, L.A., Parsons, C.H., and Kedes, D.H. (2006). Asynchronous progression through the lytic cascade and variations in intracellular viral loads revealed by high-throughput single-cell analysis of Kaposi's sarcoma-associated herpesvirus infection. J Virol. 80(20), 10073-10082. Published online 2006/09/29 DOI: 10.1128/JVI.01156-06.

Adler, H., Messerle, M., Wagner, M., and Koszinowski, U.H. (2000). Cloning and mutagenesis of the murine gammaherpesvirus 68 genome as an infectious bacterial artificial chromosome. J Virol. 74(15), 6964-6974. Published online 2000/07/11.

Ahn, J.W., Powell, K.L., Kellam, P., and Alber, D.G. (2002). Gammaherpesvirus lytic gene expression as characterized by DNA array. J Virol. 76(12), 6244-6256. Published online 2002/05/22 DOI: 10.1128/jvi.76.12.6244-6256.2002.

Avraham, R., Haseley, N., Brown, D., Penaranda, C., Jijon, H.B., Trombetta, J.J., Satija, R., Shalek, A.K., Xavier, R.J., Regev, A., et al. (2015). Pathogen Cell-to-Cell Variability Drives Heterogeneity in Host Immune Responses. Cell. 162(6), 1309-1321. Published online 2015/09/08 DOI: 10.1016/j.cell.2015.08.027.

Barton, E., Mandal, P., and Speck, S.H. (2011). Pathogenesis and host control of gammaherpesviruses: lessons from the mouse. Annu Rev Immunol. 29, 351-397. Published online 2011/01/12 DOI: 10.1146/annurev-immunol-072710-081639.

Bhatt, A.P., Wong, J.P., Weinberg, M.S., Host, K.M., Giffin, L.C., Buijnink, J., van Dijk, E., Izumiya, Y., Kung, H.J., Temple, B.R., et al. (2016). A viral kinase mimics S6 kinase to enhance cell proliferation. Proc Natl Acad Sci U S A. 113(28), 7876-7881. Published online 2016/06/28 DOI: 10.1073/pnas.1600587113.

Cesarman, E. (2014). Gammaherpesviruses and lymphoproliferative disorders. Annu Rev Pathol. 9, 349-372. Published online 2013/10/12 DOI: 10.1146/annurev-pathol-012513-104656.

Chang, P.C., Campbell, M., and Robertson, E.S. (2016). Human Oncogenic Herpesvirus and Post-translational Modifications - Phosphorylation and SUMOylation. Front Microbiol. 7, 962. Published online 2016/07/06 DOI: 10.3389/fmicb.2016.00962.

Chaturvedi, S., Klein, J., Vardi, N., Bolovan-Fritts, C., Wolf, M., Du, K., Mlera, L., Calvert, M., Moorman, N.J., Goodrum, F., et al. (2020). A Molecular Mechanism for Probabilistic Bet-hedging and its Role in Viral Latency. bioRxiv. DOI: https://doi.org/10.1101/2020.05.14.096560.

Cheng, B.Y., Zhi, J., Santana, A., Khan, S., Salinas, E., Forrest, J.C., Zheng, Y., Jaggi, S., Leatherwood, J., and Krug, L.T. (2012). Tiled microarray identification of novel viral transcript structures and distinct transcriptional profiles during two modes of productive murine gammaherpesvirus 68 infection. J Virol. 86(8), 4340-4357. Published online 2012/02/10 DOI: 10.1128/JVI.05892-11.

Coleman, H.M., Efstathiou, S., and Stevenson, P.G. (2005). Transcription of the murine gammaherpesvirus 68 ORF73 from promoters in the viral terminal repeats. J Gen Virol. 86(Pt 3), 561-574. Published online 2005/02/22 DOI: 10.1099/vir.0.80565-0.

Covarrubias, S., Gaglia, M.M., Kumar, G.R., Wong, W., Jackson, A.O., and Glaunsinger, B.A. (2011). Coordinated destruction of cellular messages in translation complexes by the gammaherpesvirus host shutoff factor and the mammalian exonuclease Xrn1. PLoS Pathog. 7(10), e1002339. Published online 2011/11/03 DOI: 10.1371/journal.ppat.1002339.

Covarrubias, S., Richner, J.M., Clyde, K., Lee, Y.J., and Glaunsinger, B.A. (2009). Host shutoff is a conserved phenotype of gammaherpesvirus infection and is orchestrated exclusively from the cytoplasm. J Virol. 83(18), 9554-9566. Published online 2009/07/10 DOI: 10.1128/JVI.01051-09.

Damania, B., Jeong, J.H., Bowser, B.S., DeWire, S.M., Staudt, M.R., and Dittmer, D.P. (2004). Comparison of the Rta/Orf50 transactivator proteins of gamma-2-herpesviruses. J Virol. 78(10), 5491-5499. Published online 2004/04/29 DOI: 10.1128/jvi.78.10.5491-5499.2004.

Diebel, K.W., Oko, L.M., Medina, E.M., Niemeyer, B.F., Warren, C.J., Claypool, D.J., Tibbetts, S.A., Cool, C.D., Clambey, E.T., and van Dyk, L.F. (2015). Gammaherpesvirus small noncoding RNAs are bifunctional elements that regulate infection and contribute to virulence in vivo. mBio. 6(1), e01670-01614. Published online 2015/02/19 DOI: 10.1128/mBio.01670-14.

Dong, S., Forrest, J.C., and Liang, X. (2017). Murine Gammaherpesvirus 68: A Small Animal Model for Gammaherpesvirus-Associated Diseases. Adv Exp Med Biol. 1018, 225-236. Published online 2017/10/21 DOI: 10.1007/978-981-10-5765-6_14.

Drayman, N., Patel, P., Vistain, L., and Tay, S. (2019). HSV-1 single-cell analysis reveals the activation of anti-viral and developmental programs in distinct sub-populations. Elife. 8. Published online 2019/05/16 DOI: 10.7554/eLife.46339.

Ebrahimi, B., Dutia, B.M., Roberts, K.L., Garcia-Ramirez, J.J., Dickinson, P., Stewart, J.P., Ghazal, P., Roy, D.J., and Nash, A.A. (2003). Transcriptome profile of murine gammaherpesvirus-68 lytic infection. J Gen Virol. 84(Pt 1), 99-109. Published online 2003/01/21 DOI: 10.1099/vir.0.18639-0.

Forrest, J.C., and Speck, S.H. (2008). Establishment of B-cell lines latently infected with reactivation-competent murine gammaherpesvirus 68 provides evidence for viral alteration of a DNA damage-signaling cascade. J Virol. 82(15), 7688-7699. Published online 2008/05/23 DOI: 10.1128/JVI.02689-07.

Glaunsinger, B.A. (2015). Modulation of the Translational Landscape During Herpesvirus Infection. Annu Rev Virol. 2(1), 311-333. Published online 2016/03/10 DOI: 10.1146/annurev-virology-100114-054839.

Gong, D., Dai, X., Xiao, Y., Du, Y., Chapa, T.J., Johnson, J.R., Li, X., Krogan, N.J., Deng, H., Wu, T.T., et al. (2017). Virus-Like Vesicles of Kaposi's Sarcoma-Associated Herpesvirus Activate Lytic Replication by Triggering Differentiation Signaling. J Virol. 91(15). Published online 2017/05/19 DOI: 10.1128/JVI.00362-17.

Guenet, J.L. (2005). The mouse genome. Genome Res. 15(12), 1729-1740. Published online 2005/12/13 DOI: 10.1101/gr.3728305.

Hair, J.R., Lyons, P.A., Smith, K.G., and Efstathiou, S. (2007). Control of Rta expression critically determines transcription of viral and cellular genes following gammaherpesvirus infection. J Gen Virol. 88(Pt 6), 1689-1697. Published online 2007/05/09 DOI: 10.1099/vir.0.82548-0.

946 Hansen, M.M.K., Desai, R.V., Simpson, M.L., and Weinberger, L.S. (2018). Cytoplasmic
947 Amplification of Transcriptional Noise Generates Substantial Cell-to-Cell Variability. Cell Syst.
948 7(4), 384-397 e386. Published online 2018/09/24 DOI: 10.1016/j.cels.2018.08.002.

949 Hartenian, E., Gilbertson, S., Federspiel, J.D., Cristea, I.M., and Glaunsinger, B.A. (2020).
950 RNA decay during gammaherpesvirus infection reduces RNA polymerase II occupancy of host
951 promoters but spares viral promoters. PLoS Pathog. 16(2), e1008269. Published online
952 2020/02/08 DOI: 10.1371/journal.ppat.1008269.

953 Hartenian, E., and Glaunsinger, B.A. (2019). Feedback to the central dogma: cytoplasmic
954 mRNA decay and transcription are interdependent processes. Crit Rev Biochem Mol Biol.
955 54(4), 385-398. Published online 2019/10/28 DOI: 10.1080/10409238.2019.1679083.

956 Hill, E.R., Koganti, S., Zhi, J., Megyola, C., Freeman, A.F., Palendira, U., Tangye, S.G., Farrell,
957 P.J., and Bhaduri-McIntosh, S. (2013). Signal transducer and activator of transcription 3 limits
958 Epstein-Barr virus lytic activation in B lymphocytes. J Virol. 87(21), 11438-11446. Published
959 online 2013/08/24 DOI: 10.1128/JVI.01762-13.

960 Jang, G.H., Lee, J., Kim, N.Y., Kim, J.H., Yeh, J.Y., Han, M., Ahn, S.K., Kang, H., and Lee, M.
961 (2016). Suppression of lytic replication of Kaposi's sarcoma-associated herpesvirus by
962 autophagy during initial infection in NIH 3T3 fibroblasts. Arch Virol. 161(3), 595-604. Published
963 online 2015/12/02 DOI: 10.1007/s00705-015-2698-2.

964 Johnson, L.S., Willert, E.K., and Virgin, H.W. (2010). Redefining the genetics of murine
965 gammaherpesvirus 68 via transcriptome-based annotation. Cell Host Microbe. 7(6), 516-526.
966 Published online 2010/06/15 DOI: 10.1016/j.chom.2010.05.005.

967 Kapadia, S.B., Molina, H., van Berkel, V., Speck, S.H., and Virgin, H.W.t. (1999). Murine
968 gammaherpesvirus 68 encodes a functional regulator of complement activation. J Virol. 73(9),
969 7658-7670. Published online 1999/08/10.

970 Kimball, A.K., Oko, L.M., Bullock, B.L., Nemenoff, R.A., van Dyk, L.F., and Clambey, E.T.
971 (2018). A Beginner's Guide to Analyzing and Visualizing Mass Cytometry Data. J Immunol.
972 200(1), 3-22. Published online 2017/12/20 DOI: 10.4049/jimmunol.1701494.

973 Kimball, A.K., Oko, L.M., Kaspar, R.E., van Dyk, L.F., and Clambey, E.T. (2019). High-
974 Dimensional Characterization of IL-10 Production and IL-10-Dependent Regulation during
975 Primary Gammaherpesvirus Infection. Immunohorizons. 3(3), 94-109. Published online
976 2019/07/30 DOI: 10.4049/immunohorizons.1800088.

977 Klasse, P.J. (2015). Molecular determinants of the ratio of inert to infectious virus particles.
978 Prog Mol Biol Transl Sci. 129, 285-326. Published online 2015/01/18 DOI:
979 10.1016/bs.pmbts.2014.10.012.

980 Krishnan, H.H., Naranatt, P.P., Smith, M.S., Zeng, L., Bloomer, C., and Chandran, B. (2004).
981 Concurrent expression of latent and a limited number of lytic genes with immune modulation
982 and antiapoptotic function by Kaposi's sarcoma-associated herpesvirus early during infection
983 of primary endothelial and fibroblast cells and subsequent decline of lytic gene expression. J
984 Virol. 78(7), 3601-3620. Published online 2004/03/16 DOI: 10.1128/jvi.78.7.3601-3620.2004.

985 Lee, H.R., Amatya, R., and Jung, J.U. (2015). Multi-step regulation of innate immune signaling
986 by Kaposi's sarcoma-associated herpesvirus. Virus Res. 209, 39-44. Published online
987 2015/03/23 DOI: 10.1016/j.virusres.2015.03.004.

Levine, J.H., Simonds, E.F., Bendall, S.C., Davis, K.L., Amir el, A.D., Tadmor, M.D., Litvin, O., Fienberg, H.G., Jager, A., Zunder, E.R., et al. (2015). Data-Driven Phenotypic Dissection of AML Reveals Progenitor-like Cells that Correlate with Prognosis. Cell. 162(1), 184-197. Published online 2015/06/23 DOI: 10.1016/j.cell.2015.05.047.

Ma, S.D., Hegde, S., Young, K.H., Sullivan, R., Rajesh, D., Zhou, Y., Jankowska-Gan, E., Burlingham, W.J., Sun, X., Gulley, M.L., et al. (2011). A new model of Epstein-Barr virus infection reveals an important role for early lytic viral protein expression in the development of lymphomas. J Virol. 85(1), 165-177. Published online 2010/10/29 DOI: 10.1128/JVI.01512-10.

Martinez-Guzman, D., Rickabaugh, T., Wu, T.T., Brown, H., Cole, S., Song, M.J., Tong, L., and Sun, R. (2003). Transcription program of murine gammaherpesvirus 68. J Virol. 77(19), 10488-10503. Published online 2003/09/13 DOI: 10.1128/jvi.77.19.10488-10503.2003.

Matthews, N.C., Goodier, M.R., Robey, R.C., Bower, M., and Gotch, F.M. (2011). Killing of Kaposi's sarcoma-associated herpesvirus-infected fibroblasts during latent infection by activated natural killer cells. Eur J Immunol. 41(7), 1958-1968. Published online 2011/04/22 DOI: 10.1002/eji.201040661.

Messinger, J.E., Dai, J., Stanland, L.J., Price, A.M., and Luftig, M.A. (2019). Identification of Host Biomarkers of Epstein-Barr Virus Latency IIb and Latency III. mBio. 10(4). Published online 2019/07/04 DOI: 10.1128/mBio.01006-19.

Nawandar, D.M., Wang, A., Makielski, K., Lee, D., Ma, S., Barlow, E., Reusch, J., Jiang, R., Wille, C.K., Greenspan, D., et al. (2015). Differentiation-Dependent KLF4 Expression Promotes Lytic Epstein-Barr Virus Infection in Epithelial Cells. PLoS Pathog. 11(10), e1005195. Published online 2015/10/03 DOI: 10.1371/journal.ppat.1005195.

Nealy, M.S., Coleman, C.B., Li, H., and Tibbetts, S.A. (2010). Use of a virus-encoded enzymatic marker reveals that a stable fraction of memory B cells expresses latency-associated nuclear antigen throughout chronic gammaherpesvirus infection. J Virol. 84(15), 7523-7534. Published online 2010/05/21 DOI: 10.1128/JVI.02572-09.

Niemeyer, B.F., Oko, L.M., Medina, E.M., Oldenburg, D.G., White, D.W., Cool, C.D., Clambey, E.T., and van Dyk, L.F. (2018). Host Tumor Suppressor p18(INK4c) Functions as a Potent Cell-Intrinsic Inhibitor of Murine Gammaherpesvirus 68 Reactivation and Pathogenesis. J Virol. 92(6). Published online 2018/01/05 DOI: 10.1128/JVI.01604-17.

O'Grady, T., Feswick, A., Hoffman, B.A., Wang, Y., Medina, E.M., Kara, M., van Dyk, L.F., Flemington, E.K., and Tibbetts, S.A. (2019). Genome-wide Transcript Structure Resolution Reveals Abundant Alternate Isoform Usage from Murine Gammaherpesvirus 68. Cell Rep. 27(13), 3988-4002 e3985. Published online 2019/06/27 DOI: 10.1016/j.celrep.2019.05.086.

Oko, L.M., Kimball, A.K., Kaspar, R.E., Knox, A.N., Coleman, C.B., Rochford, R., Chang, T., Alderete, B., van Dyk, L.F., and Clambey, E.T. (2019). Multidimensional analysis of Gammaherpesvirus RNA expression reveals unexpected heterogeneity of gene expression. PLoS Pathog. 15(6), e1007849. Published online 2019/06/06 DOI: 10.1371/journal.ppat.1007849.

Pavlova, I., Lin, C.Y., and Speck, S.H. (2005). Murine gammaherpesvirus 68 Rta-dependent activation of the gene 57 promoter. Virology. 333(1), 169-179. Published online 2005/02/15 DOI: 10.1016/j.virol.2004.12.021.

Pellett, P.J., and Roizman, B. (2013). *Herpesviridae*. In: Fields Virology.

Pfaffl, M.W. (2001). A new mathematical model for relative quantification in real-time RT-PCR. Nucleic Acids Res. 29(9), e45. Published online 2001/05/09 DOI: 10.1093/nar/29.9.e45.

Purushothaman, P., Thakker, S., and Verma, S.C. (2015). Transcriptome analysis of Kaposi's sarcoma-associated herpesvirus during de novo primary infection of human B and endothelial cells. J Virol. 89(6), 3093-3111. Published online 2015/01/02 DOI: 10.1128/JVI.02507-14.

Rochford, R., Lutzke, M.L., Alfinito, R.S., Clavo, A., and Cardin, R.D. (2001). Kinetics of murine gammaherpesvirus 68 gene expression following infection of murine cells in culture and in mice. J Virol. 75(11), 4955-4963. Published online 2001/05/03 DOI: 10.1128/JVI.75.11.4955-4963.2001.

Ruiz, J.C., Hunter, O.V., and Conrad, N.K. (2019). Kaposi's sarcoma-associated herpesvirus ORF57 protein protects viral transcripts from specific nuclear RNA decay pathways by preventing hMTR4 recruitment. PLoS Pathog. 15(2), e1007596. Published online 2019/02/21 DOI: 10.1371/journal.ppat.1007596.

Sen, N., Mukherjee, G., Sen, A., Bendall, S.C., Sung, P., Nolan, G.P., and Arvin, A.M. (2014). Single-cell mass cytometry analysis of human tonsil T cell remodeling by varicella zoster virus. Cell Rep. 8(2), 633-645. Published online 2014/07/22 DOI: 10.1016/j.celrep.2014.06.024.

Shaffer, S.M., Dunagin, M.C., Torborg, S.R., Torre, E.A., Emert, B., Krepler, C., Beqiri, M., Sproesser, K., Brafford, P.A., Xiao, M., et al. (2017). Rare cell variability and drug-induced reprogramming as a mode of cancer drug resistance. Nature. 546(7658), 431-435. Published online 2017/06/14 DOI: 10.1038/nature22794.

Shnayder, M., Nachshon, A., Krishna, B., Poole, E., Boshkov, A., Binyamin, A., Maza, I., Sinclair, J., Schwartz, M., and Stern-Ginossar, N. (2018). Defining the Transcriptional Landscape during Cytomegalovirus Latency with Single-Cell RNA Sequencing. mBio. 9(2). Published online 2018/03/15 DOI: 10.1128/mBio.00013-18.

Smiley, J.R. (2004). Herpes simplex virus virion host shutoff protein: immune evasion mediated by a viral RNase? J Virol. 78(3), 1063-1068. Published online 2004/01/15 DOI: 10.1128/jvi.78.3.1063-1068.2004.

Suarez, A.L., and van Dyk, L.F. (2008). Endothelial cells support persistent gammaherpesvirus 68 infection. PLoS Pathog. 4(9), e1000152. Published online 2008/09/13 DOI: 10.1371/journal.ppat.1000152.

Tarakanova, V.L., Leung-Pineda, V., Hwang, S., Yang, C.W., Matatall, K., Basson, M., Sun, R., Piwnica-Worms, H., Sleckman, B.P., and Virgin, H.W.t. (2007). Gamma-herpesvirus kinase actively initiates a DNA damage response by inducing phosphorylation of H2AX to foster viral replication. Cell Host Microbe. 1(4), 275-286. Published online 2007/11/17 DOI: 10.1016/j.chom.2007.05.008.

van Dyk, L.F., Virgin, H.W.t., and Speck, S.H. (2000). The murine gammaherpesvirus 68 v-cyclin is a critical regulator of reactivation from latency. J Virol. 74(16), 7451-7461. Published online 2000/07/25 DOI: 10.1128/jvi.74.16.7451-7461.2000.

Van Skike, N.D., Minkah, N.K., Hogan, C.H., Wu, G., Benziger, P.T., Oldenburg, D.G., Kara, M., Kim-Holzapfel, D.M., White, D.W., Tibbetts, S.A., et al. (2018). Viral FGARAT ORF75A

promotes early events in lytic infection and gammaherpesvirus pathogenesis in mice. PLoS Pathog. 14(2), e1006843. Published online 2018/02/02 DOI: 10.1371/journal.ppat.1006843.

Virgin, H.W.t., Latreille, P., Wamsley, P., Hallsworth, K., Weck, K.E., Dal Canto, A.J., and Speck, S.H. (1997). Complete sequence and genomic analysis of murine gammaherpesvirus 68. J Virol. 71(8), 5894-5904. Published online 1997/08/01.

Virgin, H.W.t., Presti, R.M., Li, X.Y., Liu, C., and Speck, S.H. (1999). Three distinct regions of the murine gammaherpesvirus 68 genome are transcriptionally active in latently infected mice. J Virol. 73(3), 2321-2332. Published online 1999/02/11.

Waterboer, T., Rahaus, M., and Wolff, M.H. (2002). Varicella-zoster virus (VZV) mediates a delayed host shutoff independent of open reading frame (ORF) 17 expression. Virus Genes. 24(1), 49-56. Published online 2002/04/04 DOI: 10.1023/a:1014086004141.

Weitzman, M.D., and Fradet-Turcotte, A. (2018). Virus DNA Replication and the Host DNA Damage Response. Annu Rev Virol. 5(1), 141-164. Published online 2018/07/12 DOI: 10.1146/annurev-virology-092917-043534.

Wu, T.T., Usherwood, E.J., Stewart, J.P., Nash, A.A., and Sun, R. (2000). Rta of murine gammaherpesvirus 68 reactivates the complete lytic cycle from latency. J Virol. 74(8), 3659-3667. Published online 2000/03/23 DOI: 10.1128/jvi.74.8.3659-3667.2000.

Wyler, E., Franke, V., Menegatti, J., Kocks, C., Boltengagen, A., Praktiknjo, S., Walch-Ruckheim, B., Bosse, J., Rajewsky, N., Grasser, F., et al. (2019). Single-cell RNA-sequencing of herpes simplex virus 1-infected cells connects NRF2 activation to an antiviral program. Nat Commun. 10(1), 4878. Published online 2019/10/28 DOI: 10.1038/s41467-019-12894-z.

Zamora, M.R. (2011). DNA viruses (CMV, EBV, and the herpesviruses). Semin Respir Crit Care Med. 32(4), 454-470. Published online 2011/08/23 DOI: 10.1055/s-0031-1283285.

Zhang, K., Lv, D.W., and Li, R. (2019). Conserved Herpesvirus Protein Kinases Target SAMHD1 to Facilitate Virus Replication. Cell Rep. 28(2), 449-459 e445. Published online 2019/07/11 DOI: 10.1016/j.celrep.2019.04.020.

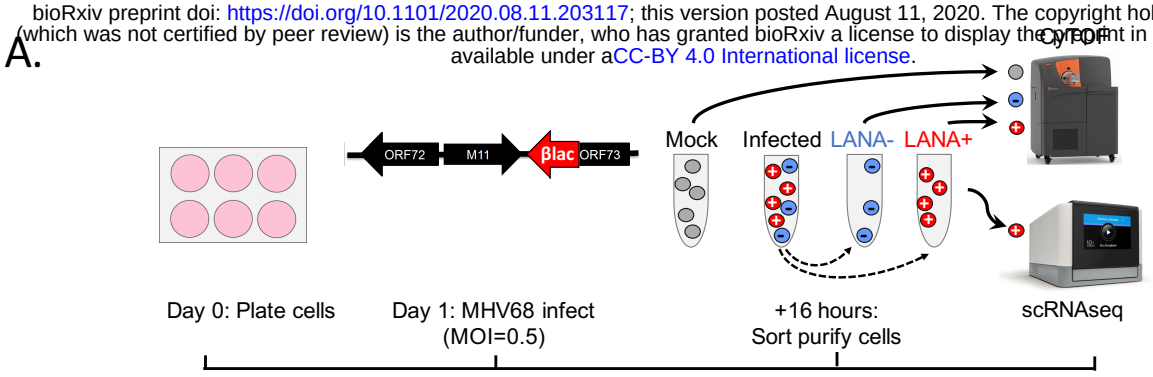

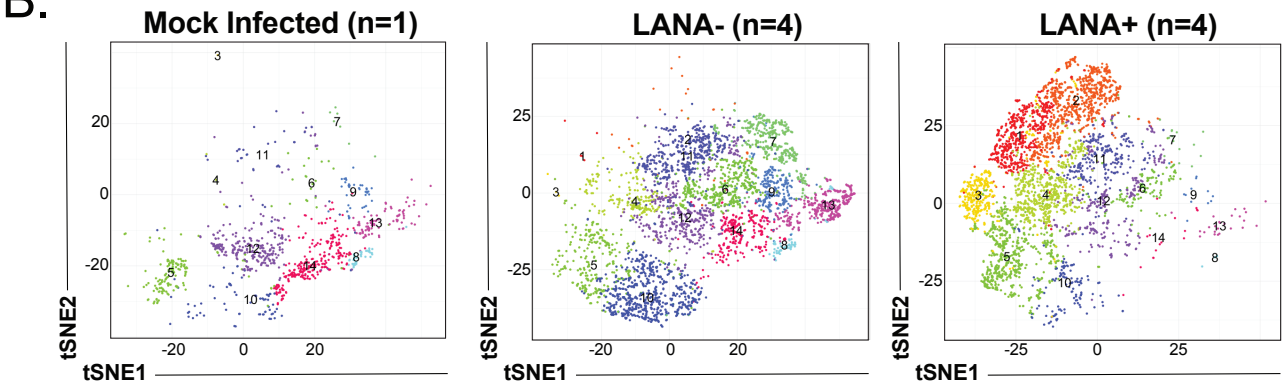

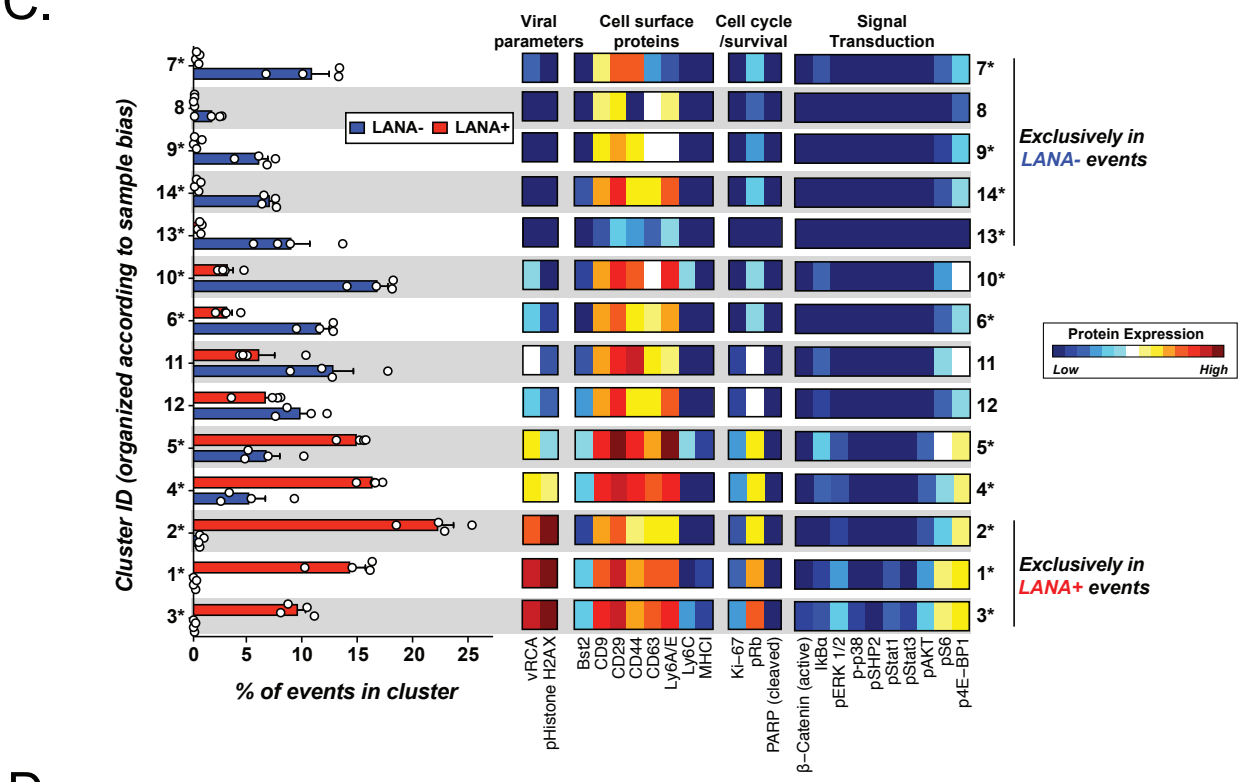

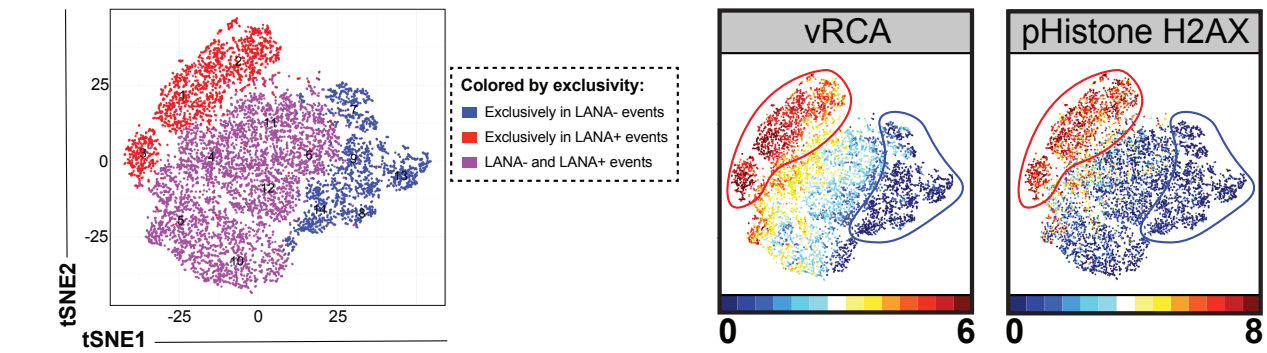

Figure 1
Berger et al

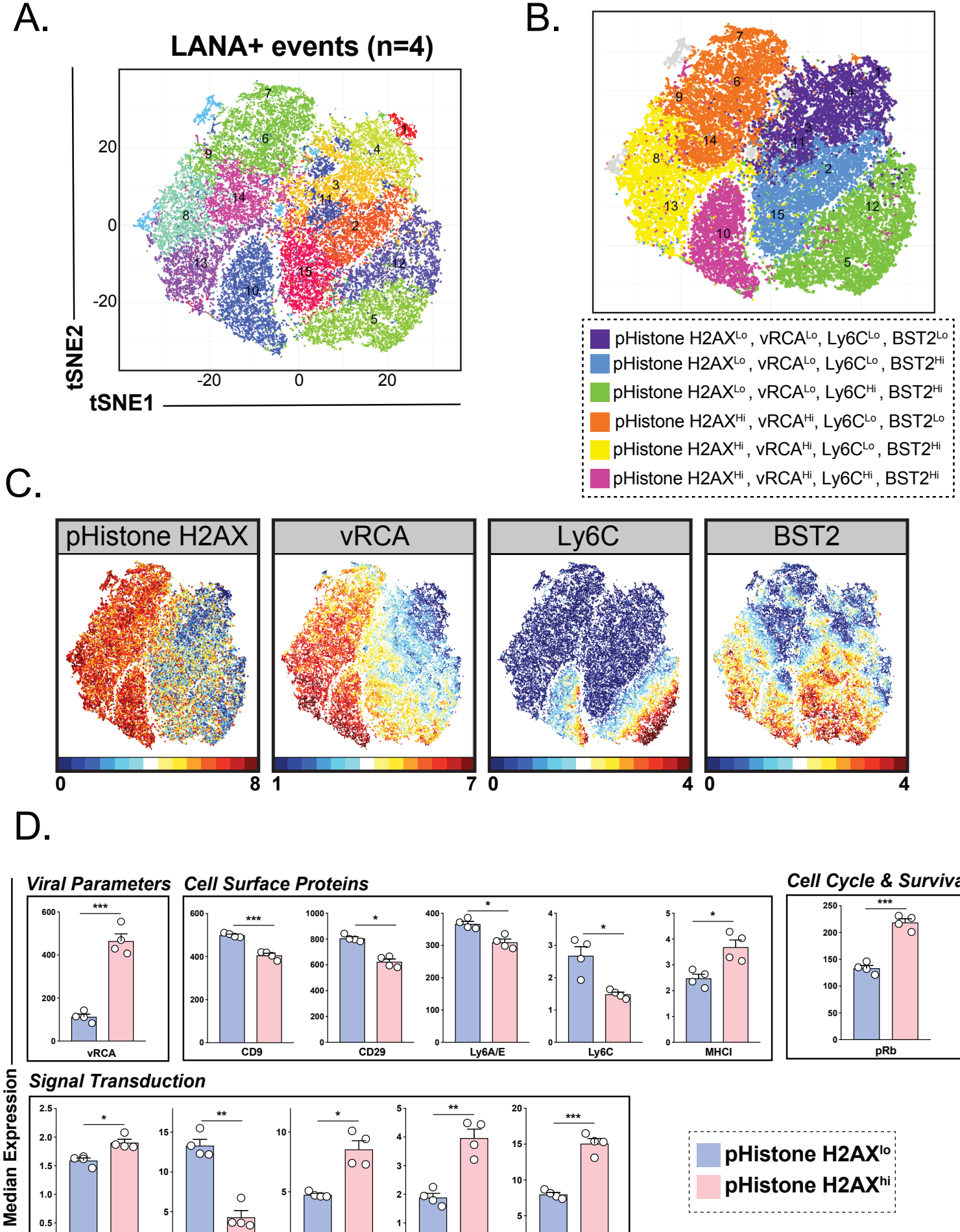

Figure 2
Berger et al

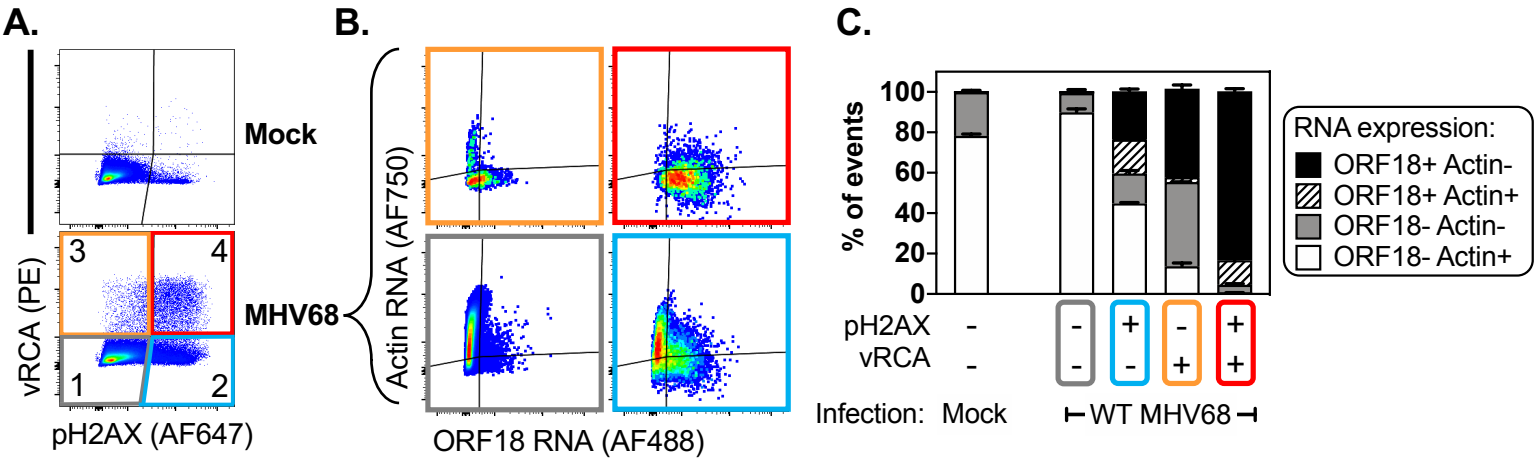

Figure 3
Berger et al

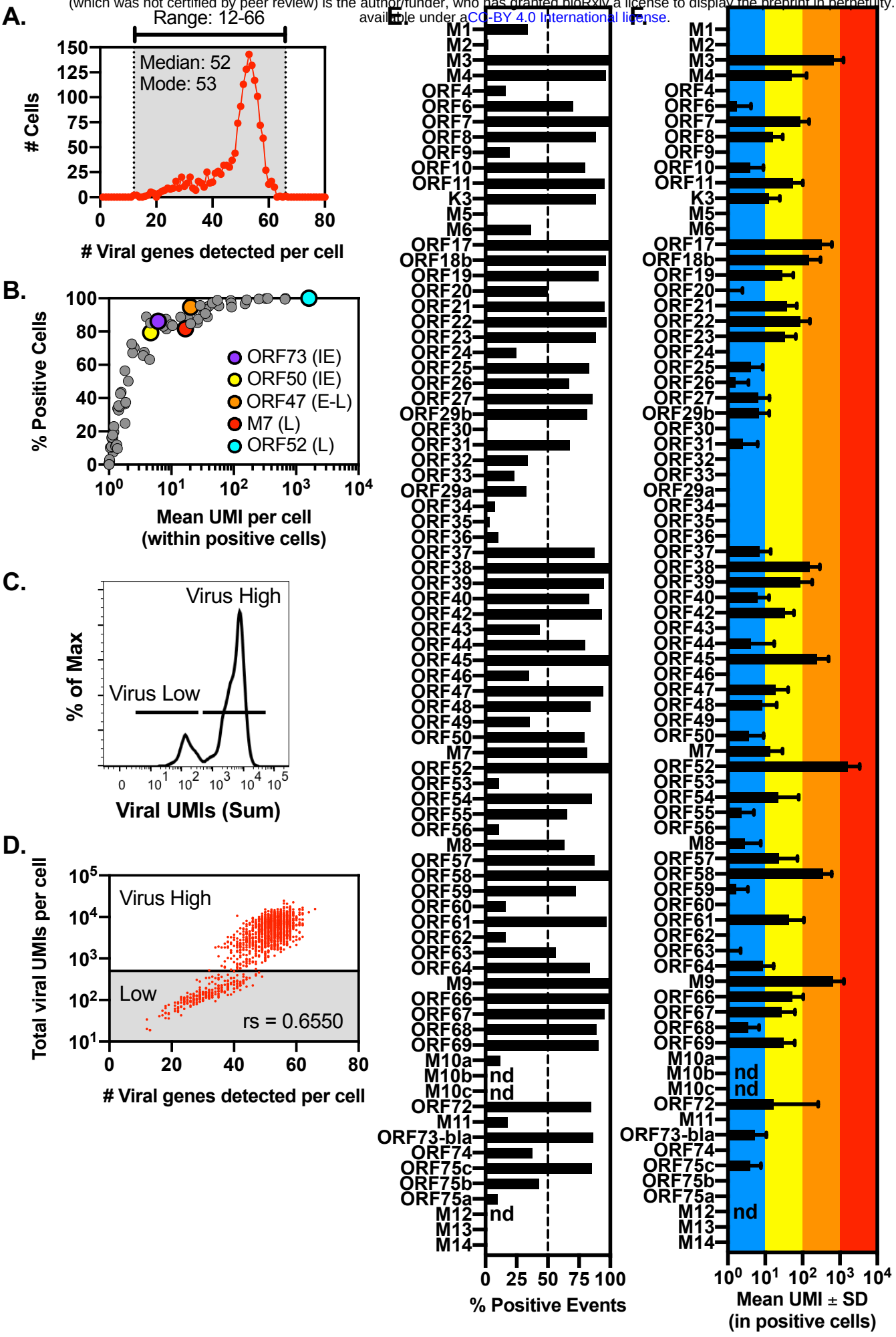

Figure 4
Berger et al

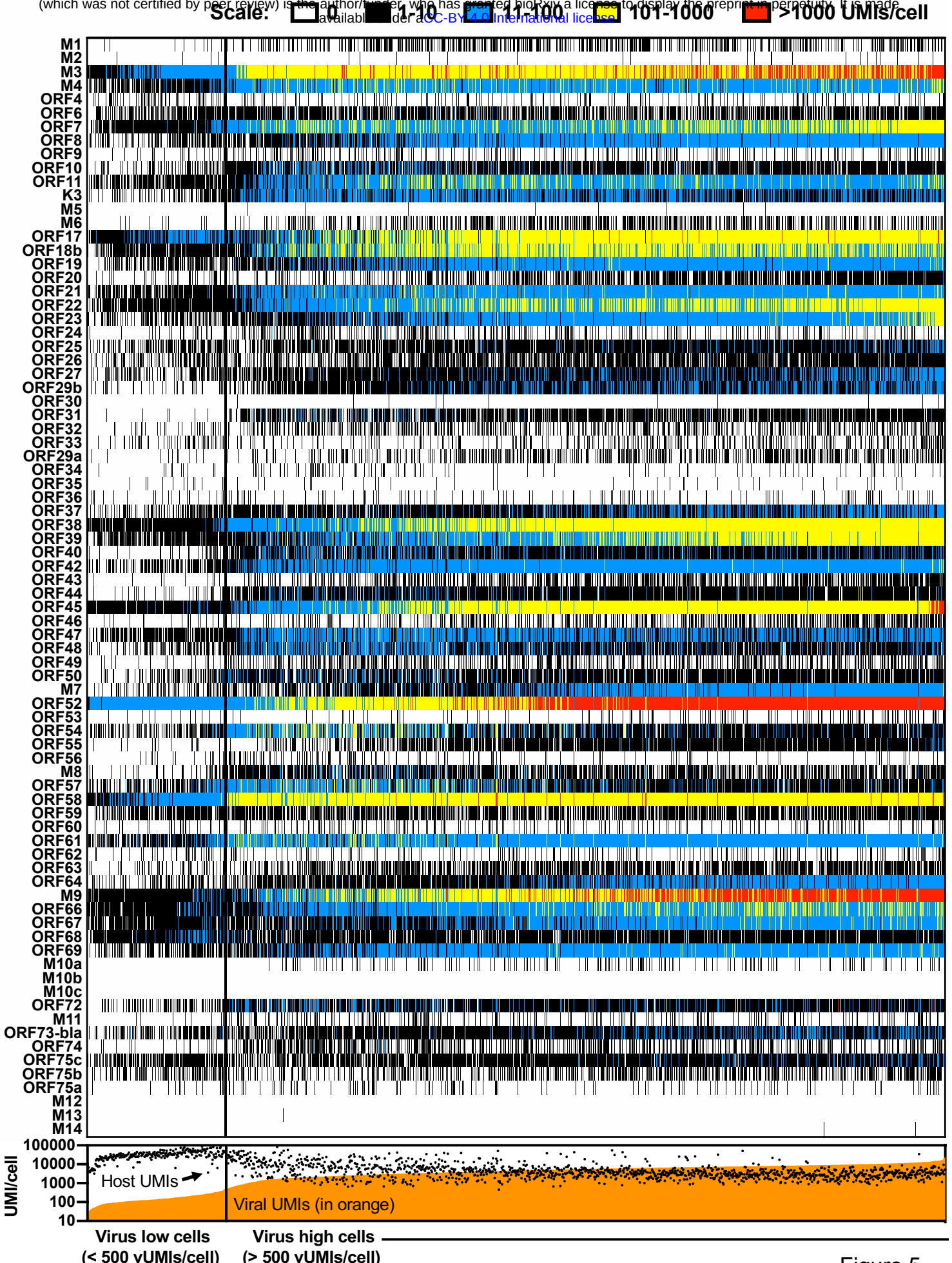

Figure 5
Berger et al

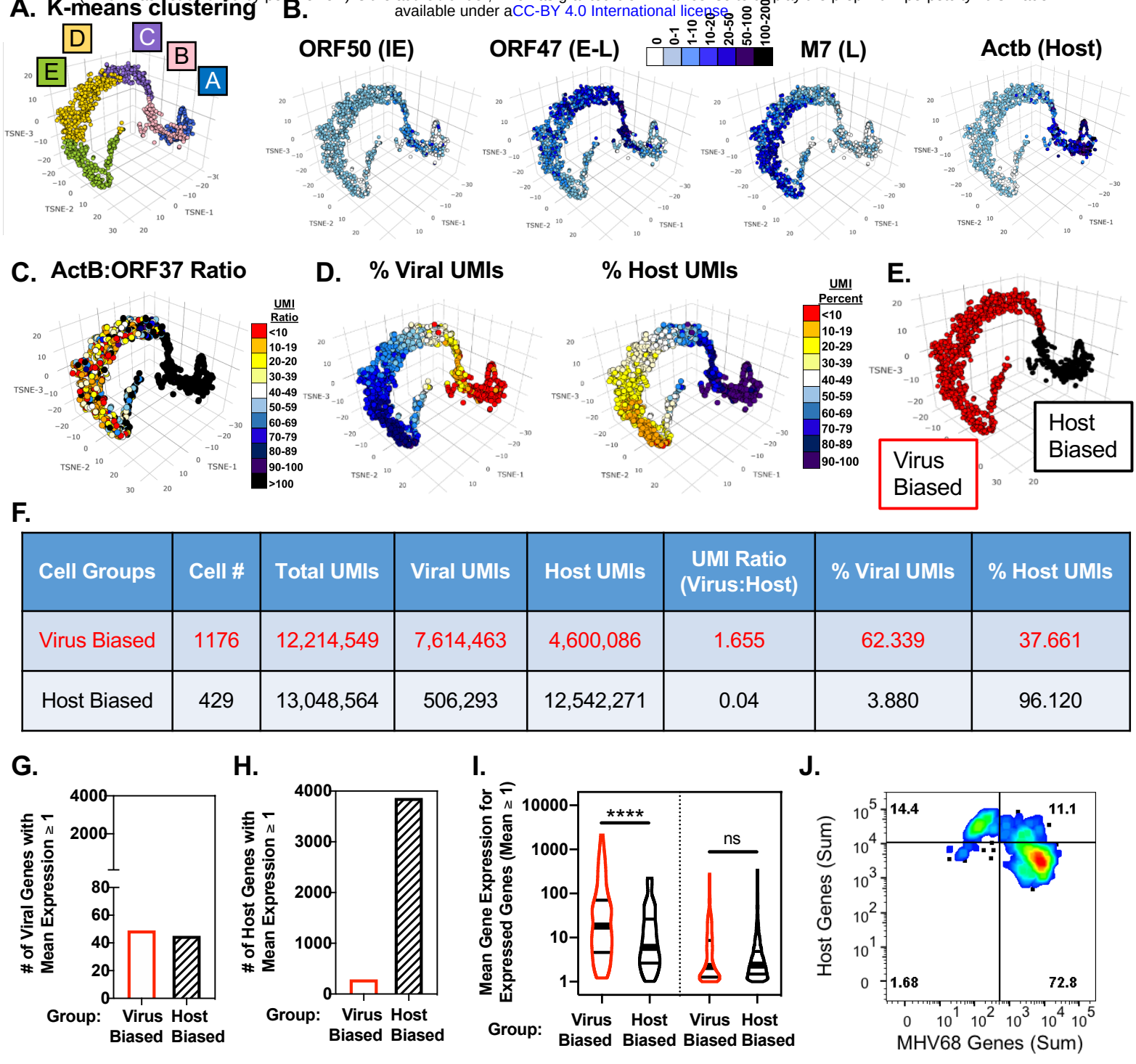

F.

Cell Groups	Cell #	Total UMIs	Viral UMIs	Host UMIs	UMI Ratio (Virus:Host)	% Viral UMIs	% Host UMIs
Virus Biased	1176	12,214,549	7,614,463	4,600,086	1.655	62.339	37.661
Host Biased	429	13,048,564	506,293	12,542,271	0.04	3.880	96.120

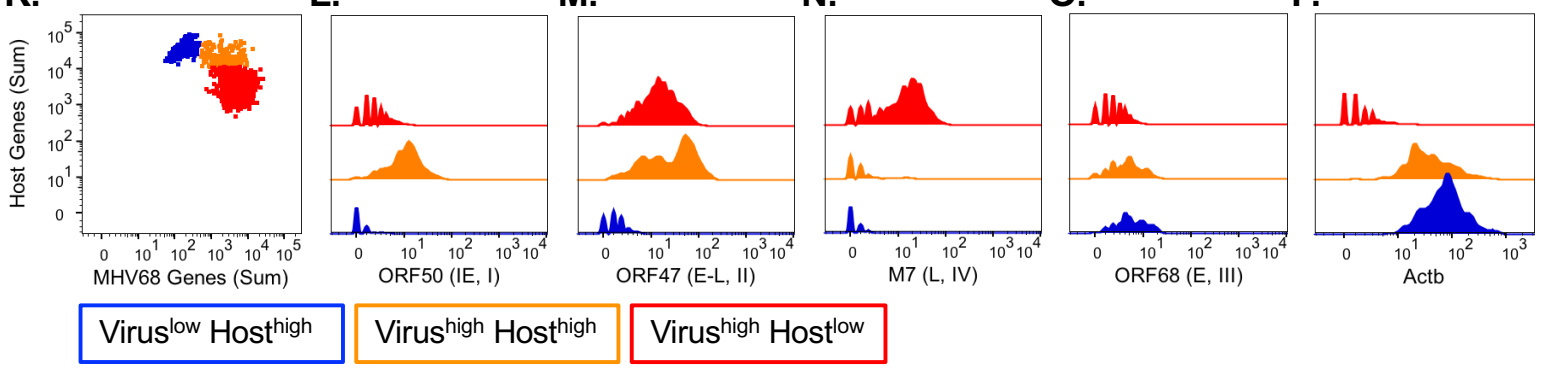

Figure 6
Berger et al

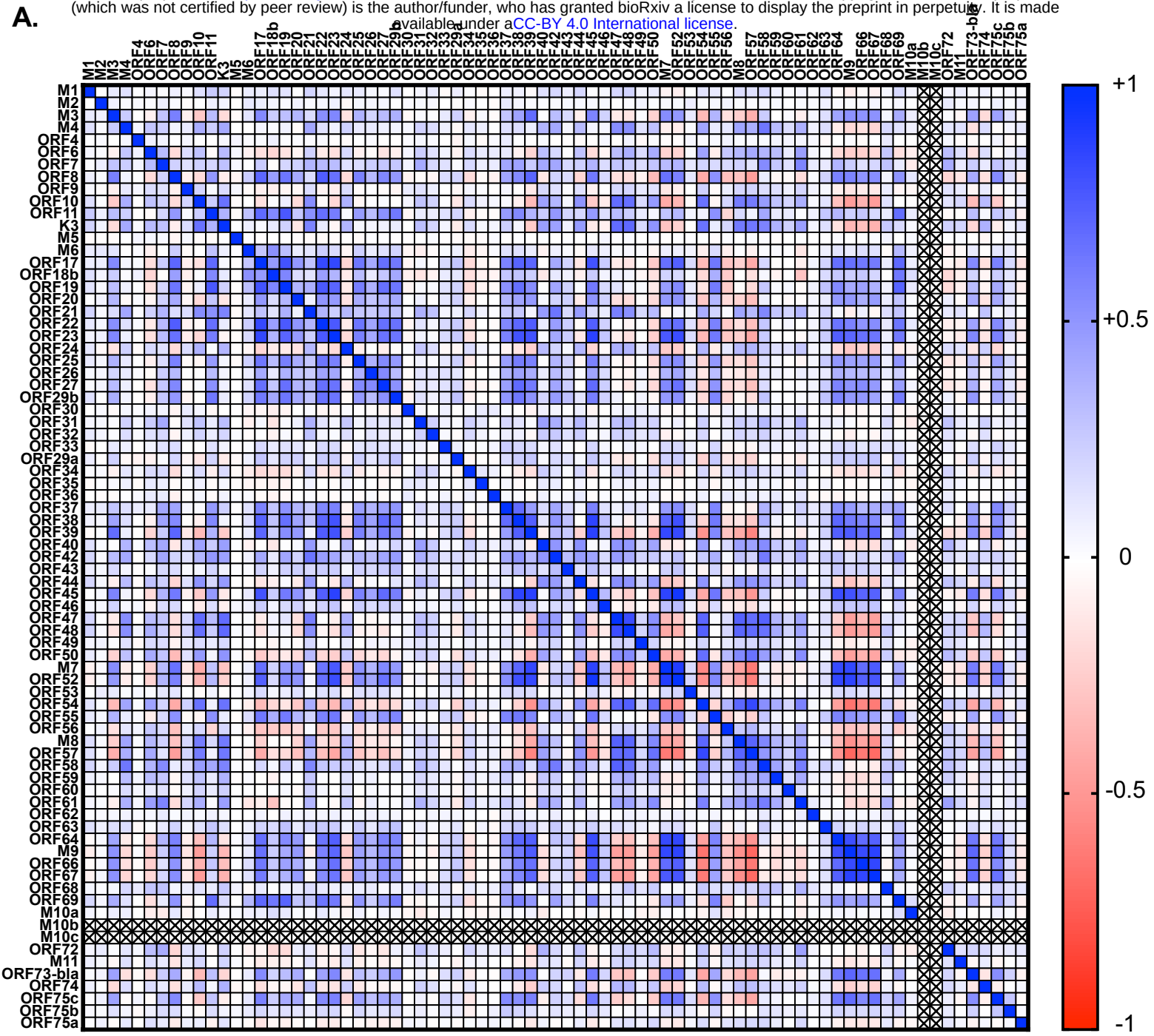

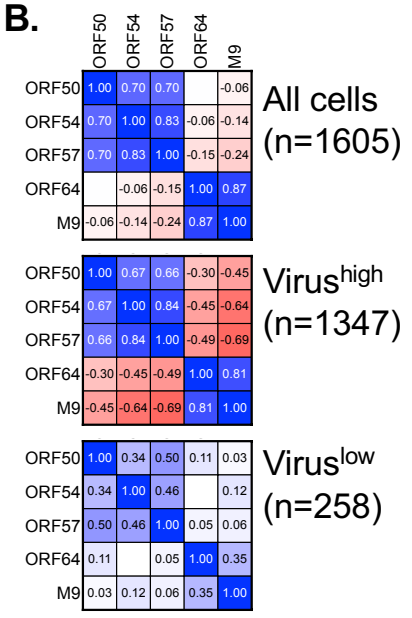

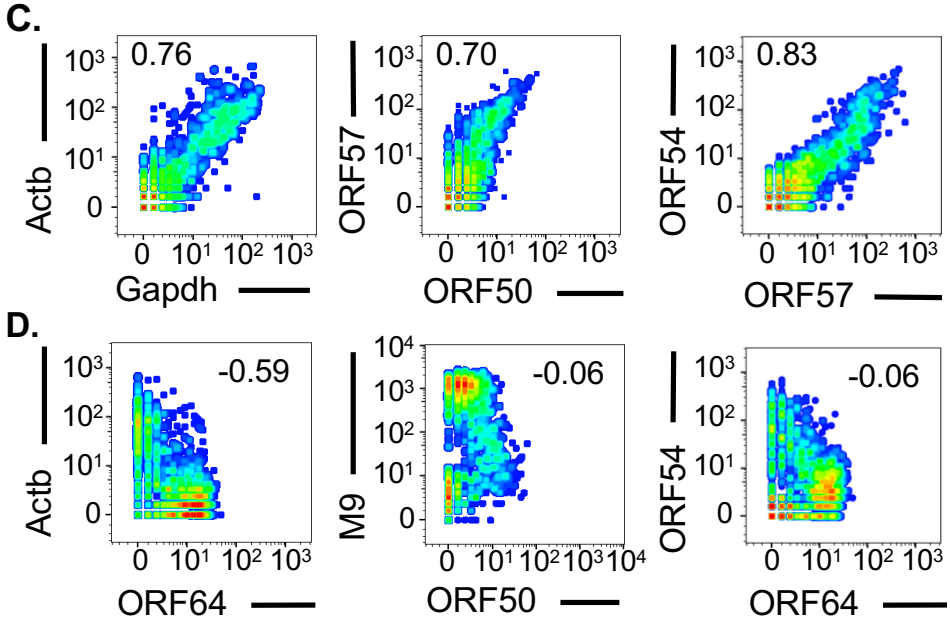

Figure 7
Berger et al